REPORT NO. DOT-TSC-FAA-73-14

L-BAND AVIONICS COMPONENTS
PERFORMANCE AND AVAILABILITY

Dr. L. F. Tami

September 1973

PRELIMINARY MEMORANDUM

1. Report No. DOT-TSC-FAA-73-14	2. Government Accession No.	3. Recipient's Catalog No.
4. Title and Subtitle L-BAND AVIONICS COMPONENTS PERFORMANCE AND AVAILABILITY		5. Report Date September 1973
		6. Performing Organization Code
7. Author's) Dr. L. F. Tami		8. Performing Organization Report No. DOT-TSC-FAA-73-14
9. Performing Organization Name and Address Department of Transportation Transportation Systems Center Kendall Square Cambridge MA 02142		10. Work Unit No. (TRAIS) R-3153/FA325
		11. Contract or Grant No.
12. Sponsoring Agency Name and Address US Department of Transportation Federal Aviation Administration Systems Research and Development Service Washington DC 20591		13. Type of Report and Period Covered Preliminary Memorandum
		14. Sponsoring Agency Code

15. Supplementary Notes

16. Abstract

The availability and performance of L-band avionics equipment was investigated for possible future use in the AEROSAT experiments on communications, surveillance, and navigation. The purpose was to review technology pertinent to low-noise pre-amplifiers, power amplifiers, antennas, and the voice-and-data modems which could be employed for an aircraft-satellite link.

17. Key Words Pre-Amplifiers Power Amplifiers L-Band Antennas Voice and Data Modems	18. Distribution Statement THIS DOCUMENT CONTAINS PRELIMINARY IN-FORMATION SUBJECT TO CHANGE. IT IS CON-SIDERED AN INTERNAL TSC WORKING PAPER WITH A SELECT DISTRIBUTION. IT IS NOT A FORMAL REFERABLE REPORT. DISTRIBUTION IS EFFECTED BY AND RESPONSIBILITY OF THE AUTHOR.		
19. Security Classif. (of this report) Unclassified	20. Security Classif. (of this page) Unclassified	21. No. of Pages 96	22. Price

Form DOT F 1700.7 (8-72)

FOR OFFICIAL USE ONLY

TABLE OF CONTENTS

iii

TABLE OF CONTENTS (CONTINUED)

ILLUSTRATIONS

ILLUSTRATIONS (CONTINUED)

ILLUSTRATIONS (CONTINUED)

LIST OF TABLES

1. LOW-NOISE PRE-AMPLIFIERS

1.1 INTRODUCTION

The purpose of this report is to describe the state-of-the-art Low-Noise Pre-Amplifiers, the developing technology of Power Amplifiers, the available L-Band Antennas for Aircraft-Satellite Links, and the performance of available Voice Modems.

1.2 GENERAL CONSIDERATIONS

Because of the low level of the down-link communications carriers as they are received by the airplane's antenna, a low-noise pre-amplifier at the L-band frequency is required to ensure low threshold performance. Sufficient gain at low-noise temperature is required to ensure that the noise contribution of mixers, line drivers, etc., on the input carrier-to-noise ratio (C/No) is negligible.

The criteria which are important to the selection of a pre-amplifier for the Satellite and the Airplane terminals are as follows:

- Noise Temperature (Noise Figure)
- Dynamic Range
- Reliability
- Cost

Four basic types of low-noise amplifiers can be considered for this application:

- Tunnel Diode Amplifiers (TDAs)
- Transistor Amplifiers
- Traveling Wave Tubes (TWTs)
- Parametric Amplifiers (Paramps)

1

Only the transistor amplifiers and parametric amplifiers will be discussed briefly. Investigations of the other two types of amplifiers have shown that they are inferior in all criteria and therefore, they are not included in this report.

1.2.1 Comparison of Low-Noise Devices

Table 1 shows the two devices with reference to the criteria mentioned in the General considerations.

TABLE 1 LOW-NOISE PRE-AMPLIFIERS

General Considerations	Transistors	Parametric Amplifiers
Noise Figure (Figure 4)	3.1 to 5.0 dB	1.0 to 2.0 dB
Cost	Low	Moderate
Dynamic Range	High	High
Reliability	High	High

From Table 1, it is obvious that the transistor amplifier is the most obvious choice for the low-noise pre-amplifier on the basis of cost, reliability, dynamic range, size, etc. Recent developments in parametric amplifiers, however, place them in much closer contention than in the past.

Uncooled paramp designs are now available with all-solid-state construction, Gunn diode pump sources, and low-noise figures at very reasonable prices. It is anticipated that a 1540 MHz uncooled paramp could be produced, with a 1.3 dB noise figure (100°K noise temperature), for a cost of about $1600.

The final choice, then, must be made on the basis of a trade-off between cost and noise figure.

The cost of Avantek Pre-Amplifiers in small quantities and for a 25 dB gain and a noise figure of 3.1 dB is about $1500 each, while for the same gain and a noise figure of 5.0 dB the price is

2

about $1000 each. The typical dynamic range is between -110 dBm and -48 dBm and is a function of the noise figure, the gain, the bandwidth, and the power involved. The calculated MTBF is between 5×10^4 and 10^5 hours.

The cost of the Parametric Amplifiers depends mainly on the bandwidth and for small quantities is about $4000 each. The dynamic range depends upon the bandwidth of the receiver which follows it. For a bandwidth of 5 MHz the dynamic range is between -40 dBm and -114 dBm. The calculated MTBF is 20,000 hours.

1.2.2 Installation and Other Constraints

System Noise Temperature considerations dictate that the loss between the antenna and the pre-amplifier be kept to a minimum. This requires that the pre-amplifier be collocated with the antenna. If more than one antenna is required, then a pre-amplifier must be associated with each antenna. This will obviously magnify the price difference between transistor and parametric pre-amplifiers.

1.2.3 Recommended Alternatives

The choice between transistor amplifiers and parametric amplifiers for the low-noise pre-amplifier is not clear at this time. Continuous advances are being made in the technology of both devices, and firm prices cannot be quoted until detailed specifications have been developed which take the environmental conditions into account.

One example each of a transistor amplifier and a parametric amplifier are given in the following paragraphs. It must be emphasized that these are examples only, and although they are produced by companies with wide experience and reputation in their respective fields, other examples could have been chosen.

1.2.4 Typical Transistor Pre-Amplifier

Transistor Amplifiers

Current techniques in the production of low-noise microwave transistors result in noise figures of 2.5 to 3.0 dB at 1540 MHz, as shown in Figure 1. Amplifiers containing these transistors are currently in production with noise figures of 3.1 to 3.6 dB at 1540 MHz, at prices in the region of $1500. In quantity production (at least 100 units) this price would drop to $500 - 800 by 1974. Transistor amplifiers of this type have a large dynamic range and excellent reliability.

The example chosen to typify the state of the transistor pre-amplifier art is the Avantek Type AS-61 which was developed under a U.S. DOT/TSC previous R&D Contract (TSC-4). Microstrip circuitry is used for the RF portion of the circuit and standard printed circuit techniques for the integral power supply. The unit is small and light, and because of the solid-state circuitry, small size and encapsulation, the amplifiers are extremely rugged, and are therefore better able to meet the general environmental requirements of MIL-E-5400.

Two transistor types were found to give equivalent noise performance in the band of interest. Both the AT-601 and the AT-101 transistors had device noise figures of 2.5 to 2.6 dB at 1.6 GHz. Noise figure and gain versus collector current for the two types are shown in Figure 2. Note that the gain shown is measured at the same source impedance that gives optimum noise figure. The maximum available gains of the device, measured by simultaneously matching input and output, are several dB higher.

The AT-101 is a production device. Its lowest noise figure occurs at a collector current of 2 to 3 mA, while maximum gain is achieved at 7 to 8 mA. The AT-601 is a developmental device with finer fingers and a larger active area than the AT-101. Its noise figure and gain optimize at slightly higher currents. Either type would have been satisfactory for use in the first stage of the amplifier, but the AT-601 was chosen for the following reasons.

4
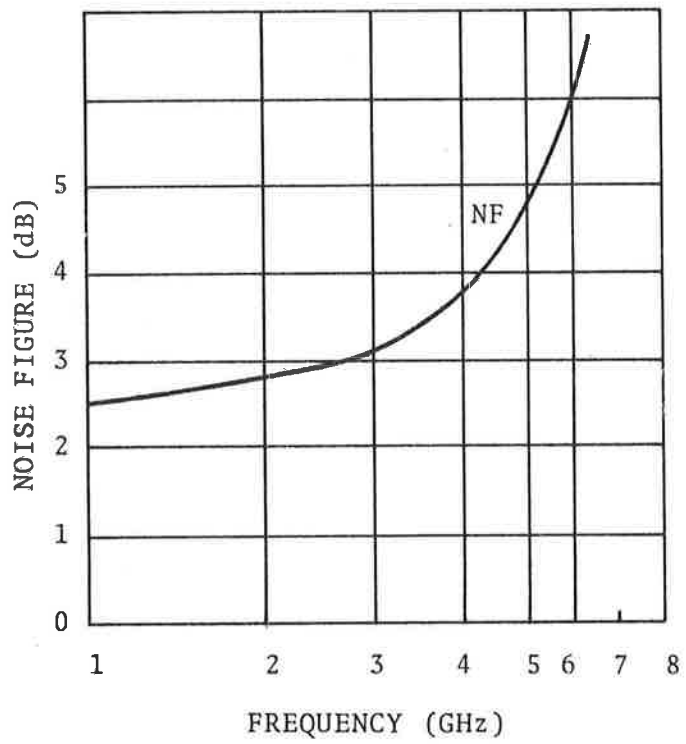
Figure 1. Noise Figure of Currently Available Microwave
Transistors

FREQ = 1.6 GHz

V_{cB} = 10V

Figure 2. Noise Figure and Gain Versus Collector Current
(Transistors AT-101 and AT-601)
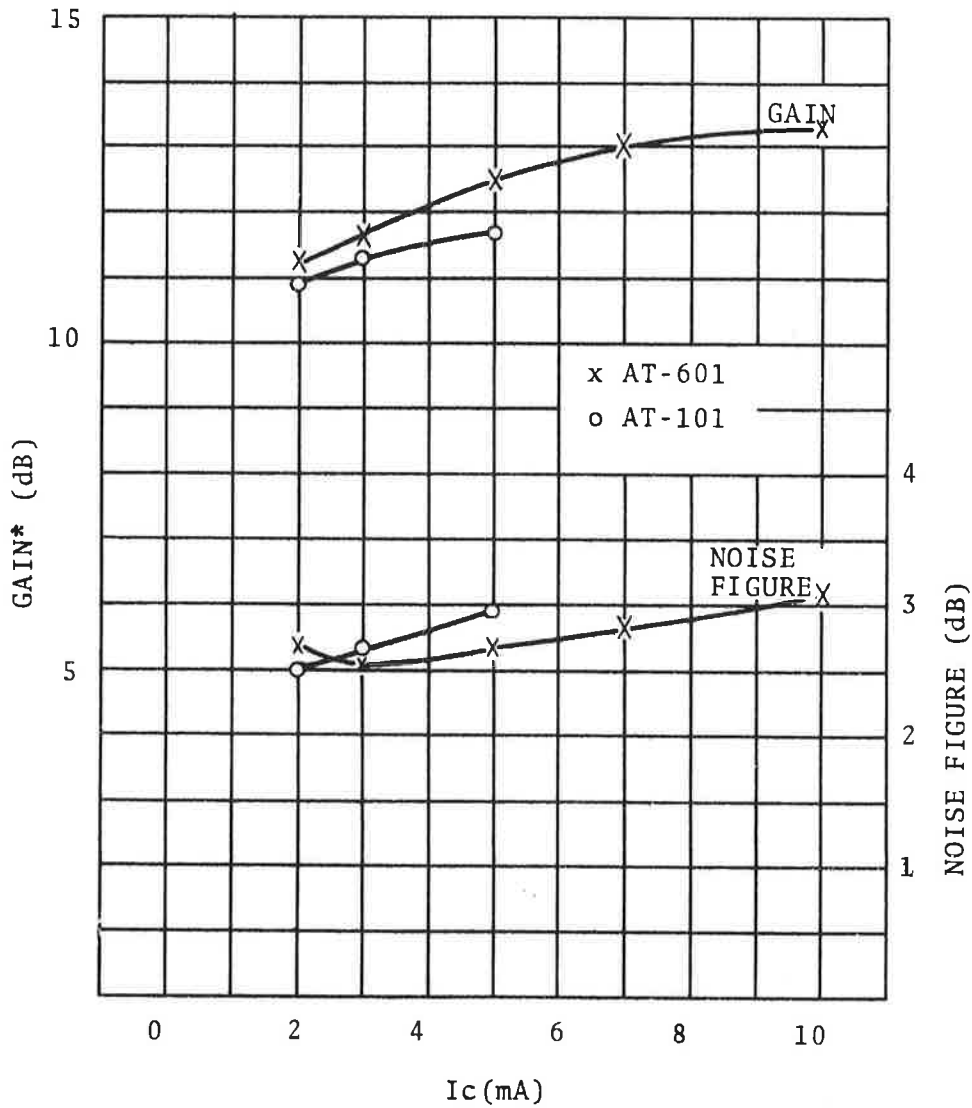
*NOTE - GAIN IS MEASURED WITH SOURCE IMPEDANCE
WHICH GIVES MINIMUM NOISE FIGURE. THE
OUTPUT IS MATCHED FOR MAXIMUM GAIN

6

a) The AT-601 provided more gain under optimum noise figure conditions. This allowed the design of the two-stage, rather than a three-stage, amplifier to meet the 23-dB minimum gain requirement of the contract.

b) Its noise figure optimized at a higher current which was useful in meeting contractual dynamic range requirements.

c) In production it is anticipated that the AT-601 will provide consistently lower noise figures than the AT-101.

Even lower noise figures (2.8 to 3.0 dB) can be achieved with another device: AT-201.

Device noise figures of 2.3 to 2.4 dB were attained with a few selected transistors. The AT-201 has approximately the same active area as the AT-601 combined with the geometry, or "finger width," of the AT-101. The decreased noise figure was achieved by the development of new diffusions which raised the f_T of the AT-201 to about 6 GHz.

Figure 3 presents a comparison of the new AT-201 with the AT-601. Two of the new devices were used in the front end of one of the U.S. DOT/TSC prototype amplifiers; i.e., Model AS-61.

1.3 AMPLIFIER DESIGN

A block diagram of the final amplifier design is presented in Figure 4. The unit consists of a balanced input stage, followed by a single-ended output stage. The balanced input stage is of the type described by K. Kurokowa.[3] It employs two 3-dB 90° hybrid couplers and two single-ended amplifiers. Theoretically, the combination has the same gain and noise figure as a single-ended amplifier.

1.4 RECOMMENDATIONS

Advances made in the course of this project clearly point to the possibility of significantly improved noise-figure performance in the very near future. Avantek transistor engineers are confident that they can optimize a transistor for a noise figure of 1.8 dB

7
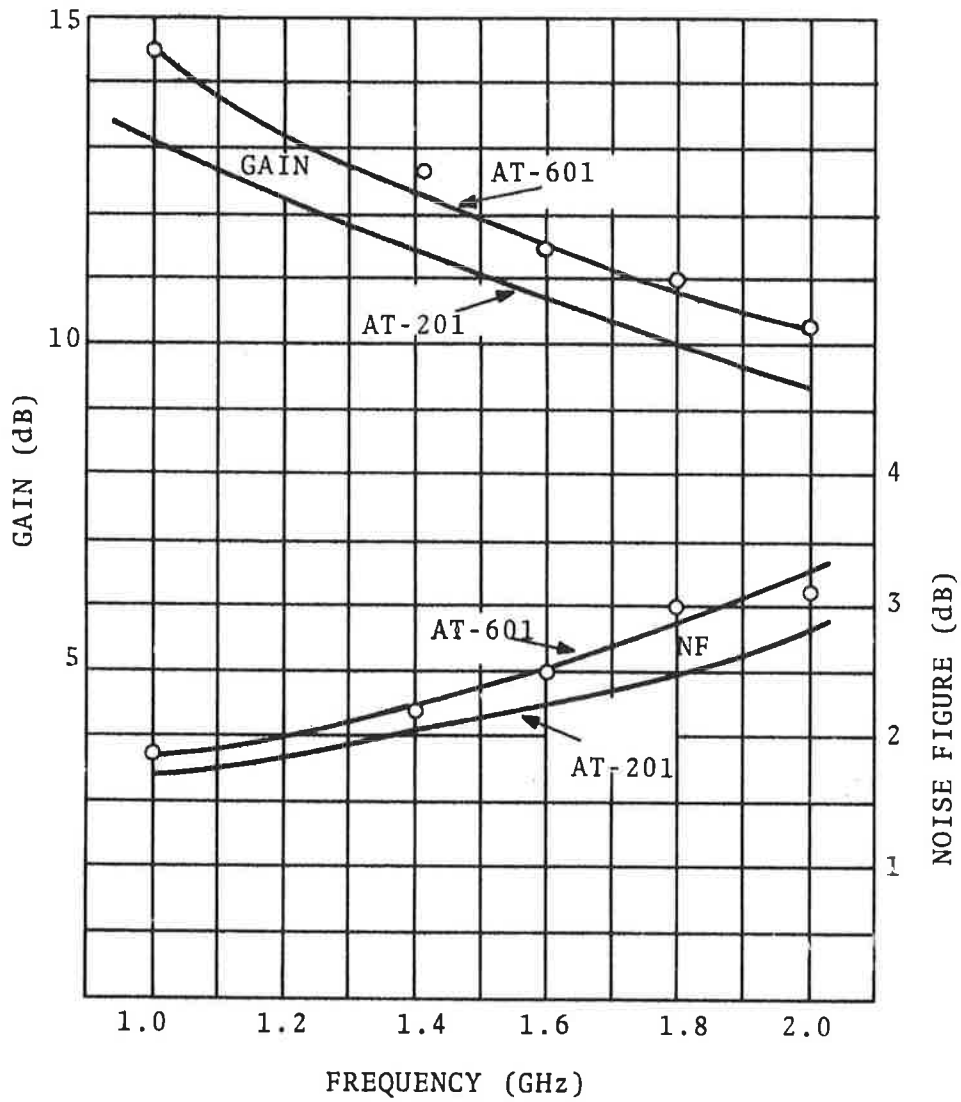
Figure 3. Comparison of Transistor AT-201 with Transistor AT-601

8
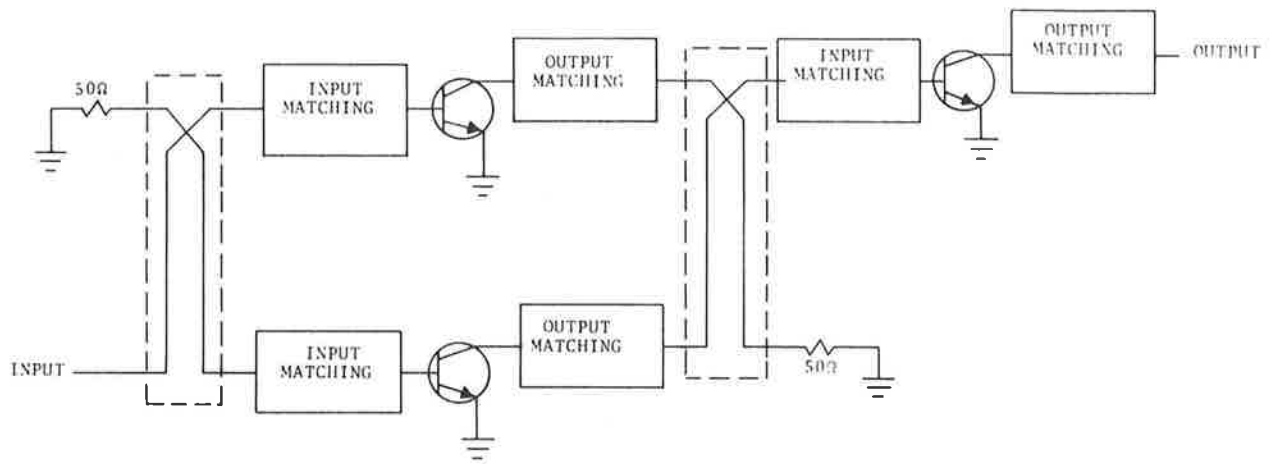
Figure 4.   Block Diagram of Final Amplifier Design

9

at 1.6 GHz. A transistor of this type would produce an amplifier with a 2.5-dB noise figure met over the 1.45 to 1.66 GHz frequency range. However, this cannot be achieved without a development contract.

NOTE

Other manufacturers, as listed in Table 2, have also verified that a Noise Figure of less than 2.5 dB is obtainable in the range 1.7 GHz to 2 GHz. These devices inherently operate as well or better at the lower bands of interest, namely 1.535 GHz to 1.66 GHz.

TABLE 2   NOISE FIGURES OF LESS THAN 2.5 dB OBTAINABLE IN
1.7 TO 2.0 GHz RANGE FOR THREE DIFFERENT DEVICES

DEVICE	2 GHz dB	1.7 GHz dB	Amplifier 290°K dB	1.7 GHz -30°C dB	Amplifier -30°C dB
Fairchild MT 4000	2.32	2.25	2.46	1.96	2.15
California Eastern Laboratory V-578	2.35	2.3	2.51	2.00	2.20
Hewlett-Packard 35862E	2.5	2.4	2.62	2.09	2.29

1.5   TYPICAL UNCOOLED PARAMETRIC AMPLIFIERS

The unit chosen to exemplify the modern uncooled paramp technology is one of the "Unipak" range developed by AIL, Inc., of Deer Park, L.I.

Compared to a transistor amplifier, a paramp is a relatively narrowband device. The Unipak range does not currently include an amplifier centered at 1550 MHz, although the range extends from 1200 MHz to over 6000 MHz. Only detailed changes to existing units of the L-band range would be required to adapt the amplifier for the 1.535 GHz to 1.66 GHz.

10

The performance characteristics of a model 9816L-1 paramp are shown in Table 3.

The amplifier uses the balanced-diode configuration developed in 1961.[4] It consists of a four-port circulator and a varactor mount. The circulator is a two-junction ferrite device with low insertion loss and high reverse isolation. The varactor mount has a coaxial signal circuit consisting of an impedance matching transformer and a series inductance which, together with the varactor diodes, forms a tuned circuit. The pump signal is provided from a 9.5-GHz Gunn diode oscillator and mixes in the varactors with the input signal. The varactors, in their mounts, are self-resonant at the difference frequency, approximately 8.2 GHz, so this frequency is sustained in the "idler" cavity. This idler frequency remixes with the predominant pump frequency to recreate the input signal frequency at a higher level than the input level. The non-linearity which causes the mixing is in a purely reactive parameter, namely the diode junction capacitance, so no thermal noise is produced by this process. The only resistive loss is in the bulk resistance of the diode semiconductor material. By cooling the diodes, noise temperatures close to absolute zero are theoretically achievable. In this application the noise temperature is about 120°K, less than half the physical temperature.

Very few components are used, and this is a mature design which is suitable for batch production in moderate quantities. The varactor mount and pump source are both temperature stabilized by resistive heaters and a fully regulated, diode bias power supply is provided. In the model illustrated, the center frequency is adjustable, and the adjustment is made by varying the diode bias voltage, which varies the capacitance and thus the self-resonant frequency of the diodes.

A more recent development, and one which would be worth pursuing if production quantities in the thousands were contemplated, is an integrated circuit paramp. Development has been undertaken in this field for some years,[5] and hardware design has progressed to the point where noise figures of less than 1.7 dB are achievable with a circuit which operates in the 2200 - 2300 MHz region.

TABLE 3   PERFORMANCE CHARACTERISTICS OF UNIPAK
MODEL 9816L-1 SOLID-STATE PARAMETRIC
AMPLIFIERS

Frequency Band:	1245 MHz - 1370 MHz, tunable
Bandwidth:	30 MHz minimum, 50 MHz typical
Gain:	20 dB ±1 dB across band
Noise Figure:	2 dB maximum, 1.5 dB typical
Saturation Point:	-40 dBm input at 1 dB compression
Operating Temperature Range:	0° C - 50° C
Input Power:	28 VDC ±20 percent, 2 amp
Size:	7 x 9 x 2 in. 178 x 249 x 51 mm
Weight:	5 lb. 2.3 kg
Operating Controls:	Single-knob frequency control

This type of amplifier could be produced with the pump source as part of the integrated circuit, so that the entire amplifier could be constructed on a single substrate. A fixed-tuned, 10-MHz bandwidth paramp with 20 dB of gain and a noise temperature of 100°K at 1550 MHz could, conceivably, be produced in quantity for less than $1000 using this technique. This is a long way from the status of five years ago.

Five years ago Klystron pumps were used which have high voltage power supplies in the order of 1000 volts. Furthermore, there were no substrate techniques truly available. The cost of Parametric Amplifiers in large quantities was about $10,000 each, but the general performance was comparable to that achieved today. Therefore, the improvements are in size, weight and cost, but not in performance.

1.6 REFERENCES

1. Final Technical Report Contract No. DOT/TSC-4 by Avantek, Inc. October 30, 1970.

2. Mendoza, B., D. Lawson, G. Herbert, and J. Luse, Maritime Services Satellite System Definition Study. Automated Marine International. July 1971.

3. Kurokowa, K., Design Theory of Balanced Transistor Amplifiers, Bell System Technical Journal, October 1965, p. 1675-1698.

4. Kliphuis, J., US Patent 3,105,941: Parametric Amplifier with Balanced Self-Resonant Diodes. May 1, 1962.

5. Cuccia, C.L., Ultra-Low-Noise Pre-Amplifiers in Satellite Earth Terminal Installations, Advances in Microwaves, Vol. 7, Academic Press, Inc., N.Y., N.Y. (1971), p. 177-283.

2. POWER AMPLIFIERS

This report is concerned with developing technology rather than standard technology. The traveling wave tubes (TWT) and the electrostatically focused Klystrons (ESK's) performance is well known and established and therefore, only solid-state power amplifiers will be described.

The choice of transmitter power amplifiers must be made on the basis of those parameters which are critical to the operation of the system. The most important of these characteristics are:

a. Output Power

b. Reliability

c. Efficiency, defined as $\dfrac{\text{RF Power Out} - \text{RF Power in}}{\text{DC Power in}} \times 100\%$,

   for a single carrier at saturation

d. Weight/Size

e. Cost.

The high-frequency power transistor art has advanced significantly during the past decade. Prior to 1962, no practical high-frequency power devices existed. Germanium, in spite of theoretical advantages, was not practical for these transistors, partly because of limitations in technology and partly because it did not permit high-temperature operation. The introduction of silicon planar technology in small-signal devices marked the beginning of microwave power transistors. Virtually all such transistors today are silicon planar n-p-n bipolar devices. Table 4 lists some typical performance figures.

TABLE 4   TYPICAL PERFORMANCE OF MICROWAVE POWER TRANSISTORS
(28-VOLT BIAS, CW, COMMON-BASE CIRCUIT)

Frequency GHz	Power watts	Gain dB	Efficiency percent
1.0	20	10	60
2.0	10	7	50
3.0	5	5	30

The microwave power transistor is a nonlinear device; the operation of a high-frequency power transistor is similar to that of the low-frequency device but requirements for dimensions, process control, heat sinking, and packaging are much more severe.

The state of the art in high-power transistor technology is limited by the geometry of the devices themselves. The upper boundaries of achievable power and frequency are being pushed back at a declining rate, and it is unlikely that the available power from a single transistor will exceed 20 watts at 1600 MHz within the next three years, except for laboratory-type devices. There is no lack of incentive, but the device manufacturers are reaching the limits of current manufacturing techniques, materials, and packaging design. A major technological breakthrough could change this picture overnight, but such an event is, of course, impossible to predict. From the curves shown in Figure 5 it is possible to extrapolate that a 1600-MHz transistor with a power output capability of 20 watts will be available by 1974. Devices at this power level are working now under laboratory conditions, but yields are low, and such devices are historically prone to catastrophic failure. It is essential that any device that is going to be operating in the airborne environment be as predictable as is possible in its operational behavior. It is obviously impractical to jeopardize the success of a multi-million dollar program by using unproven devices.
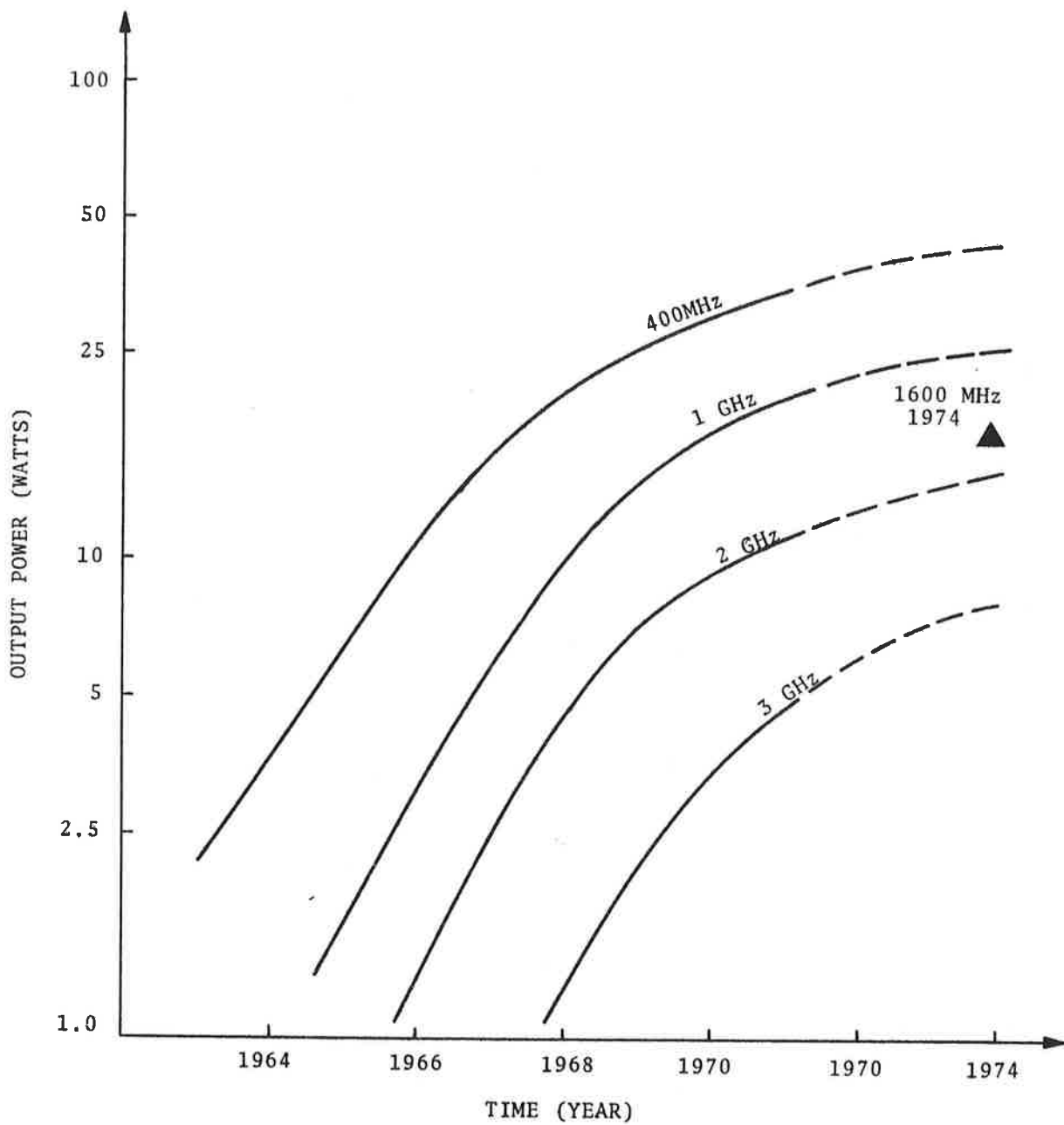
Figure 5.   Maximum R-F Power Available from Microwave Transistors

As far as size and weight are concerned, transistors appear to have a clear lead over competing devices. This, however, is only one small component of a power amplifier. A 200-watt amplifier would require approximately 24 devices with associated heat sinks, couplers, and stripline components and packages. Such an amplifier would probably weigh in excess of 8 pounds.[2]

The efficiency of transistor amplifiers at 1600 MHz is quite difficult to assess. Single devices are available with collector efficiencies of over 80% at 400 MHz. The best devices currently available at 1600 MHz have collector efficiencies of approximately 50 - 60%. It is possible to improve the efficiency of these devices, but their impedances are so low that they are difficult to match, both externally and internally, at the higher frequencies.

At 1600 MHz and higher frequencies, high power is available only in devices with relatively low gain. Typical transistors exhibit gains of the order of 7 - 10 dB. A significant amount of RF power is thus required to drive the output power stages, and this must be taken into account when calculating overall efficiencies. The efficiency of the driver stages is also of concern.

As a general rule, the collector efficiency of a microwave transistor increases as the power output is increased up to saturation, but this is by no means true of the power amplifier as a subsystem. Because of the limitations on the power output of individual devices, they must be operated in parallel to produce power levels in excess of 20 watts. The outputs of individual amplifiers must then be combined in stripline hybrid couplers. These would not necessarily be discrete components, but could be integrated into an amplifier package to minimize problems of matching and loss. It is probable, however, that the ohmic losses and, additionally, the unbalance produced by manufacturing tolerances and material inhomogeneity will result in each coupler having an attenuation of approximately 0.2 dB. Each time the number of parallel stages is doubled, therefore, the output insertion loss increases by 0.2 dB and the overall efficiency is thus reduced by about 5%.

17

As a further practical consideration, variations in power output, gain, and efficiency of individual transistors within a production batch would probably make it impossible to match (say) 16 transistors perfectly in every respect. Some designers allow as much as 1.0-dB margin for this effect and that due to performance variation over probable temperature range, but this is probably too conservative a figure. It is anticipated that improvements in device production in the next two years will permit the use of about 0.25 dB of margin for the effect of production yield variation. A block diagram of a typical transistor high power amplifier is shown in Figure 6.

A sample efficiency calculation based on this configuration is presented in Table 5. The power level chosen is quite arbitrary, but lies within the range of spacecraft capabilities detailed in the previous section. This hypothesizes a 220-watt transistor amplifier at 1540 MHz with an efficiency of 39%. The individual transistor parameters which were estimated for the power amplifier are as follows:

RF Output Power	20 watts at 1540 MHz
Maximum Gain	7.0 dB at 20 watts
Collector Efficiency	60% at maximum output, 1540 MHz

Manufacturer's data for the RCA developmental transistor TA 7994, operating at 2 GHz, are shown in Figure 7. The comparison was made at 2 GHz, rather than at 1540 MHz, because the characteristics of the devices were measured at this frequency. It can be seen from the data of Figure 7 that the gain, power output, and efficiency of these transistors are considerably lower than predicted for a 1540-MHz device. This is largely due to the very rapid decline of all three parameters with increasing frequency. Additional margin was also added to account for improvements in the future development of the devices. The results of calculations made for a 16-transistor power amplifier operating at 2 GHz, 6 watts, show that it would be slightly more efficient to operate with the
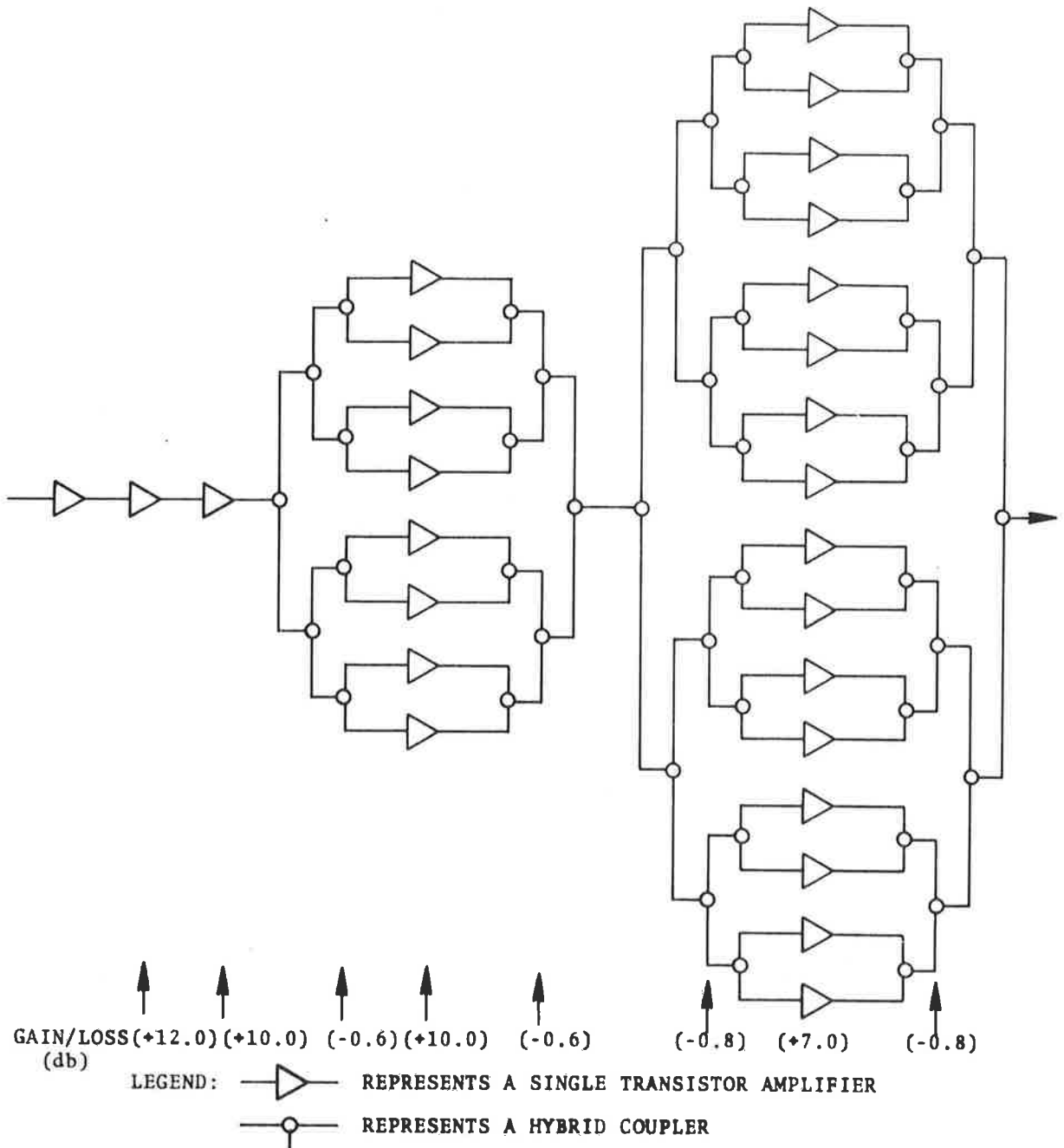
Figure 6. Block Diagram of 16-Transistor Amplifier

TABLE 5 EFFICIENCY OF 220-WATT, 16-TRANSISTOR AMPLIFIER (1540 MHz)
         Ref. 2

No.	Parameter	Value	Remarks
1	RF Power at PA Output	23.42 dBW	220 watts
2	Loss of 16-Way Combiner	0.8 dB	
3	RF Power at Final Transistor Output	24.22 dBW	1+2; 264 watts = 16.5W/ Transistor
4	Collector Efficiency (η_c)	60%	
5	DC Power to Output Stage	440 watts	3 $\div$ 4
6	Output Transistor Gain	7.0 dB	
7	Interstage Loss	1.4 dB	8-way combiner + 16-way divider
8	Net Gain from Driver Output	5.6 dB	6 - 7
9	RF Power at Driver Output	18.62 dBW	3 - 8 8 x 9.1 watts = 72.8 watts
10.	DC Power to Driver Stage	122 watts	9 $\div$ 0.6 (60% efficiency)
11	Driver Transistor Gain	10.0 dB	Gain improves at lower level
12	Interstage Loss	0.6 dB	8-way divider
13	Net Gain from Pre-driver Output	9.4 dB	
14	RF Power at Pre-driver Output	9.22 dBW	9 - 13
15	DC Power to Pre-driver Stage	13.9 watts	14 $\div$ 0.6 (60% efficiency)
16	Pre-driver Transistor Gain	10.0 dB	Same as 11.
17	RF Power at Pre-pre-driver Output	1.0 watt	No interstage
18	DC Power Required	1.3 watts	17 $\div$ 0.6
19	Estimated DC Required by Low-Level Amps	0.8 watts	
20	Total DC Power Required	578 watts	5 + 10 + 15 + 18 + 19
21	Overall Efficiency	39%	1 $\div$ 20
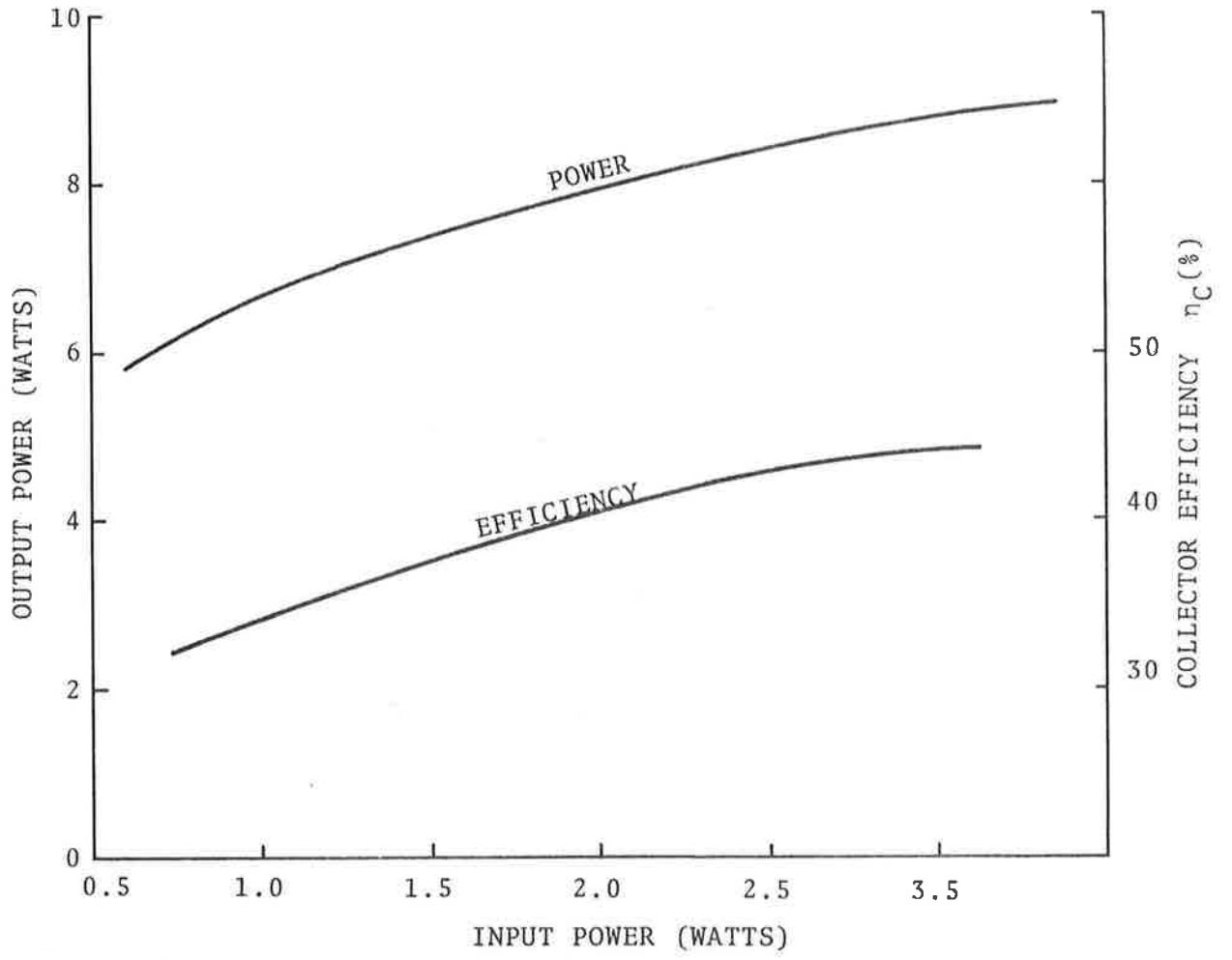
Figure 7.   RCA TA 7994 Transistor Output Power and Efficiency
Versus Input Power

larger number of transistors at the lower power level, although the collector efficiency of the output stage transistors is 10% higher at the higher power level.

This effect is due to the lower gain at the higher levels. The difference in drive power required is almost 3:1. The curve of Gain and Input Power shown in Figure 8 illustrates this phenomenon.

This conclusion is interesting, and not at all what one would expect from initial inspection of the device characteristics.

What this means in terms of system performance is that it would seem to be possible to operate with the output stages at a lower power level without incurring any penalty from loss of efficiency.

It can be concluded with some confidence, that overall efficiencies of approximately 40% will be achievable at power levels of around 100 - 200 watts and frequencies of 1535 - 1545 MHz, and the amplifiers can be operated in a sufficiently "quasi-linear" state to permit considerable improvement in Carrier to Interference ratios achievable with adjacent carriers.

Experiments with solid-state amplifiers at these frequencies indicate that a 1.0-dB back off from saturated output is sufficient to provide a Carrier to Interference ratio of 16 dB with multiple, equally spaced carriers. A further benefit to be gained from operation below saturation is that the additional unbalance caused by the amplifier non-linearity when operating with unbalanced carriers is reduced. This reduces the requirement for sophisticated power-balancing techniques in the spacecraft.

The current limitations in the technology of hybrid combining networks are restricting the usefulness of transistor amplifiers at high-power levels. As power increases, the insertion loss of the hybrid increases, and since more hybrids are required at the higher powers, the net effect is to reduce the efficiency at high-power levels. Figure 9 shows how the efficiency varies as a function of power levels for a series of amplifiers using a transistor type

22
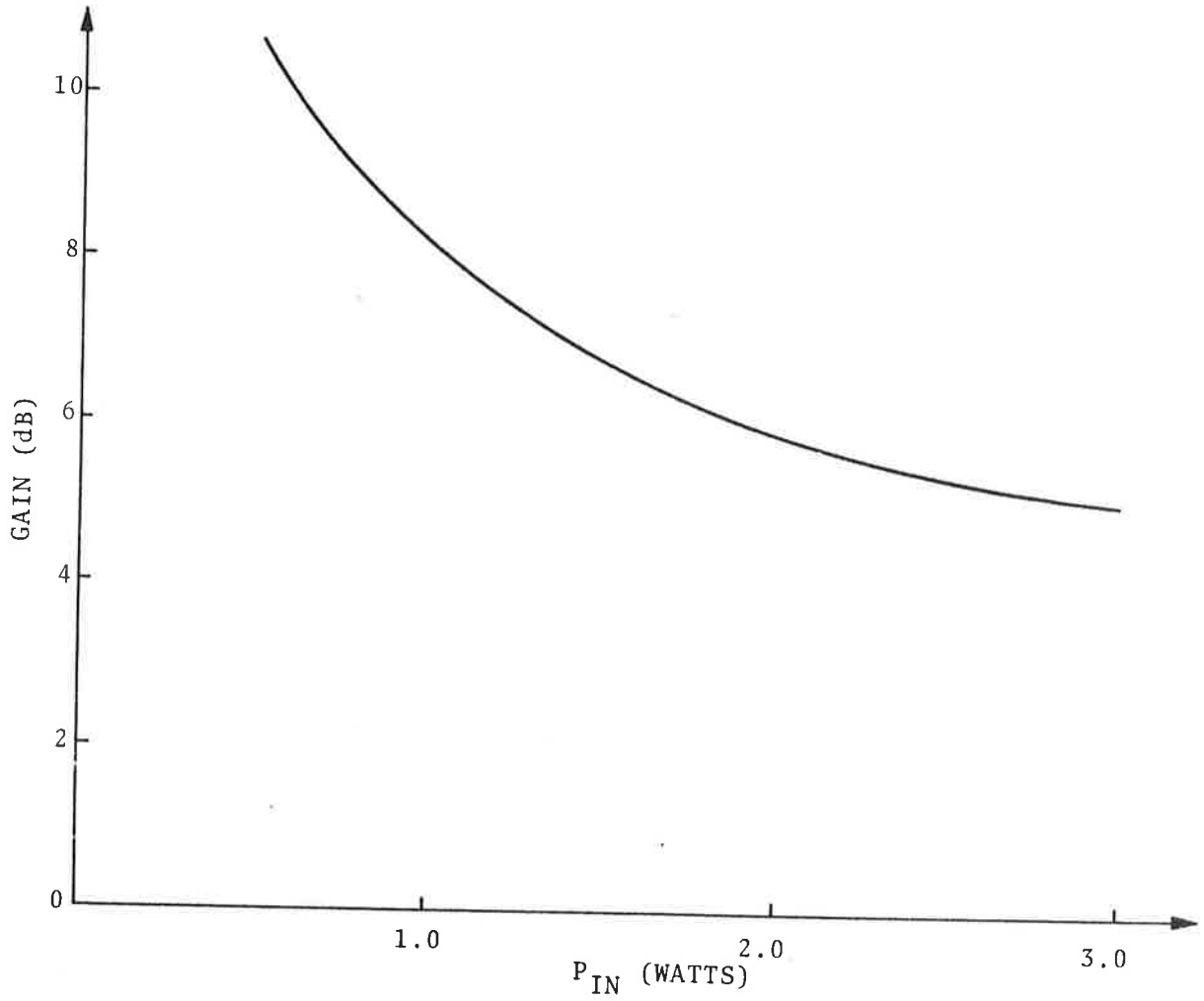
Figure 8.   Gain Versus Input Power: RCA TA 7994 at 2GHz
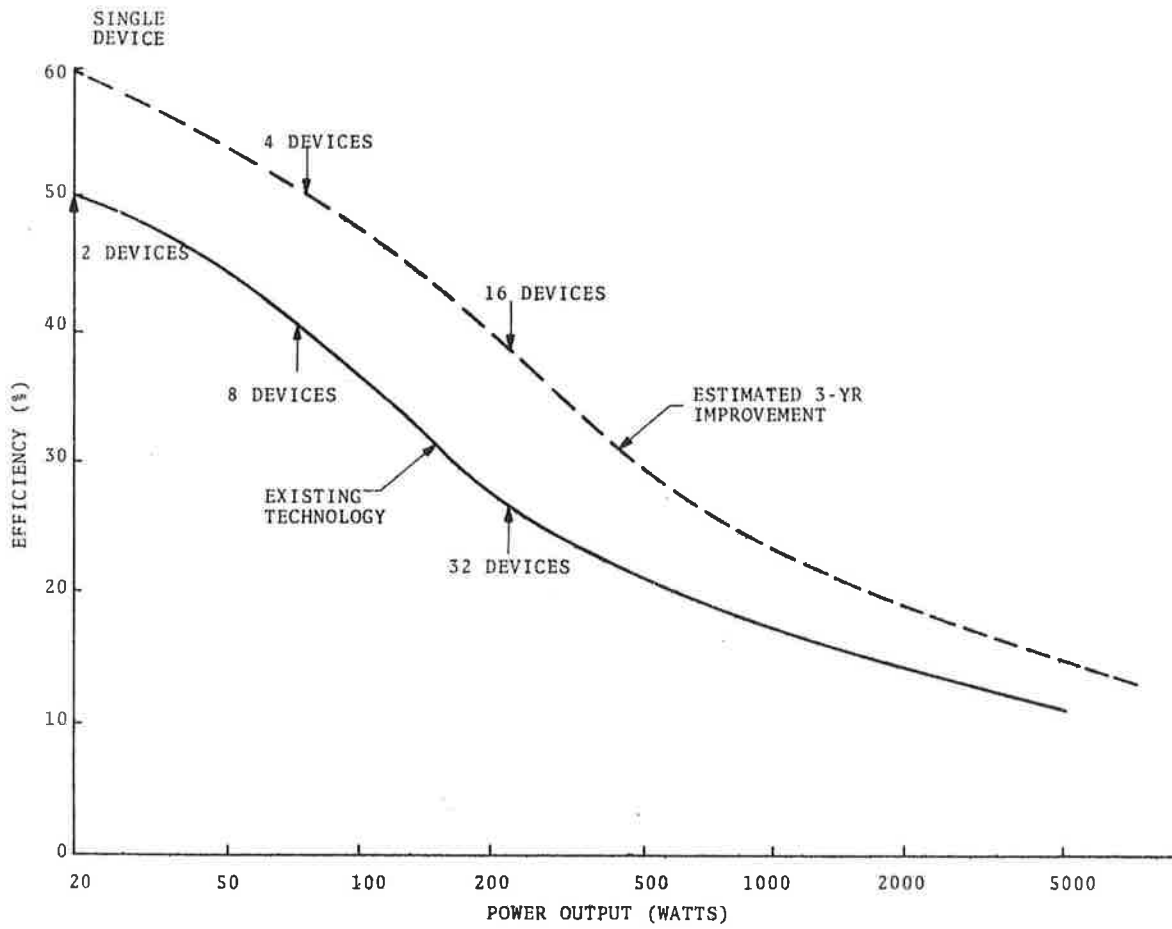
Figure 9. Transistor Amplifier Locus of Efficiency Versus Power

TABLE 6. EXAMPLES OF TYPICAL APPLICATIONS OF MICROWAVE AND SOLID-STATE DEVICES
Ref. 1

Device	Application	Advantage of Solid-State Devices over Tube	Advantage of Solid-State Used over Other Solid-State Devices
Transistor	L-band telemetry transmitters for weather sondes and gun projectile monitoring	Simple, low-voltage power supply, much smaller and more rugged than tubes (particularly important for projectile monitoring), potentially lower cost, better frequency stability	Lowest cost, moderate-power CW L-band device available
Transistor	Transmitters for L-band phased-array radars	Simple, low-voltage power supply, no warmup required, higher reliability is expected to lead to lower overall ownership cost over the life of the radar	Reliable, high-power CW L-band devices available, compact amplifier circuit since no circulators are required. Reliable class C operation (no dc pre-pulsing required)
Transistor	Transmitters for L- and S-band communications systems	Simple, low-voltage power supply, high reliability	Reliable, high-power L- and S-band devices available

with 10 watts output, 50% collector efficiency, and 10 dB of gain at 1540 MHz. From this it can be seen that the overall efficiency is well below 20% at a power level of 1 Kw. It is unlikely that development over the next three years will result in a 50% improvement in that figure, so that an optimistic figure would be 25% overall efficiency at 1 Kw.

2.1 CONCLUSIONS

Solid-state microwave power sources are being used in increasing numbers in an increasing variety of applications. A list of several representative applications is given in Table 6. Higher power devices require more research and development.

2.2 REFERENCES

1.   Sobol,H. and F. Sterzer, Microwave Power Sources, IEEE Spectrum, April 1972.

2.   Mendoza, B., D. Lawson, G. Herbert, and J. Luse, Maritime Services Satellite System Definition Study, August 1971. Automated Marine International.

3. REVIEW OF AVAILABLE L-BAND ANTENNAS FOR AIRCRAFT-SATELLITE COMMUNICATIONS LINK

3.1 INTRODUCTION

One of the problems encountered in the use of a satellite system for communications (and for surveillance and navigation) is that of finding a suitable aircraft antenna. Ideally, an aircraft-mounted antenna which could be used to communicate with at least one satellite in synchronous orbit should have the following properties:

a. Hemispherical coverage above the aircraft

b. Rejection of signals from the hemisphere below the aircraft

c. Circular polarization

d. Low aerodynamic drag

e. Simple installation on existing aircraft

f. High power-handling capability

g. High reliability, dependability, and ease of maintenance

h. Low cost.

These are not independent requirements, and there is no antenna which will simultaneously satisfy all of those requirements. The purpose of this section is to briefly review the characteristics of some of the L-band antennas which could be used for an aircraft-satellite link.

3.2 MULTIPATH REJECTION REQUIREMENTS

If the antenna pointing profile is known and the antenna gain requirement is established, then the antenna requirements are completely defined. Implicit in that statement is that in determining the antenna gain requirement, a multipath fade margin should be considered that would ensure a specified link-continuity exceeding

level, generally 99%. For antenna pointing-angles near the horizon (<5°), the required fade margin, in general, increases for a given exceeding level; hence, the difference must be accounted for by increased antenna gain or improved multipath rejection, or both. Thus, antenna pointing profile and antenna gain are not independent, but are related at low angles by requirements for rejection multipath.

Any antenna design should attempt to maximize response to the direct signal between the airplane and the satellite and exhibit a minimum response to the signal reflected from the earth's surface.

The ratio of the direct-wave gain to the reflected-wave gain at a particular angle of arrival is defined as the multipath discrimination factor. For a circularly polarized system, this multipath discrimination factor is maximized by an aircraft antenna pattern that is nearly circularly polarized for the direct path and has a high axial ratio for the reflected-wave path.

3.3 TRW CURVED TURNSTILE ANTENNA

This antenna was designed to meet the following performance criteria: near upper hemispherical coverage having high rejection to lower hemisphere signals; operating frequencies within the L-band and a bandwidth of approximately 5 MHz; antenna gain of at least 0 dBi with respect to a circularly polarized isotropic antenna over a cone area of 160°; and an axial ratio within 5 dB.

The antenna consists of two curved dipoles which are orthogonally excited by a 90° hybrid coupler to provide the circular polarization. The chief advantage of the curved dipole design as opposed to ordinary designs is that it provides a much wider pattern to a high degree of uniformity, while maintaining a good axial ratio.

A low profile Fiberglas radome can be used to protect the crossed elements of the antenna. For mechanical rigidity the radome is filled with dielectric foam by injection through a hole on the baseplate.

28

NOTE: The peak gain is 3.9 db
with respect to a circu-
lar isotropic source.
Pattern: Voltage
Frequency: 1.6 GHz
Polarization: RHC

PATTERN: VOLTAGE
FREQUENCY: 1.6 GHz
POLARIZATION: RHC
CONSTANT: Ø = 0°
VARIABLE: θ

PATTERN: VOLTAGE
FREQUENCY: 1.6 kHz
POLARIZATION: RHC
CONSTANT: Ø = 45°
VARIABLE: θ

PATTERN: VOLTAGE
FREQUENCY: 1.6 kHz
POLARIZATION: RHC
CONSTANT: Ø = 90°
VARIABLE: θ
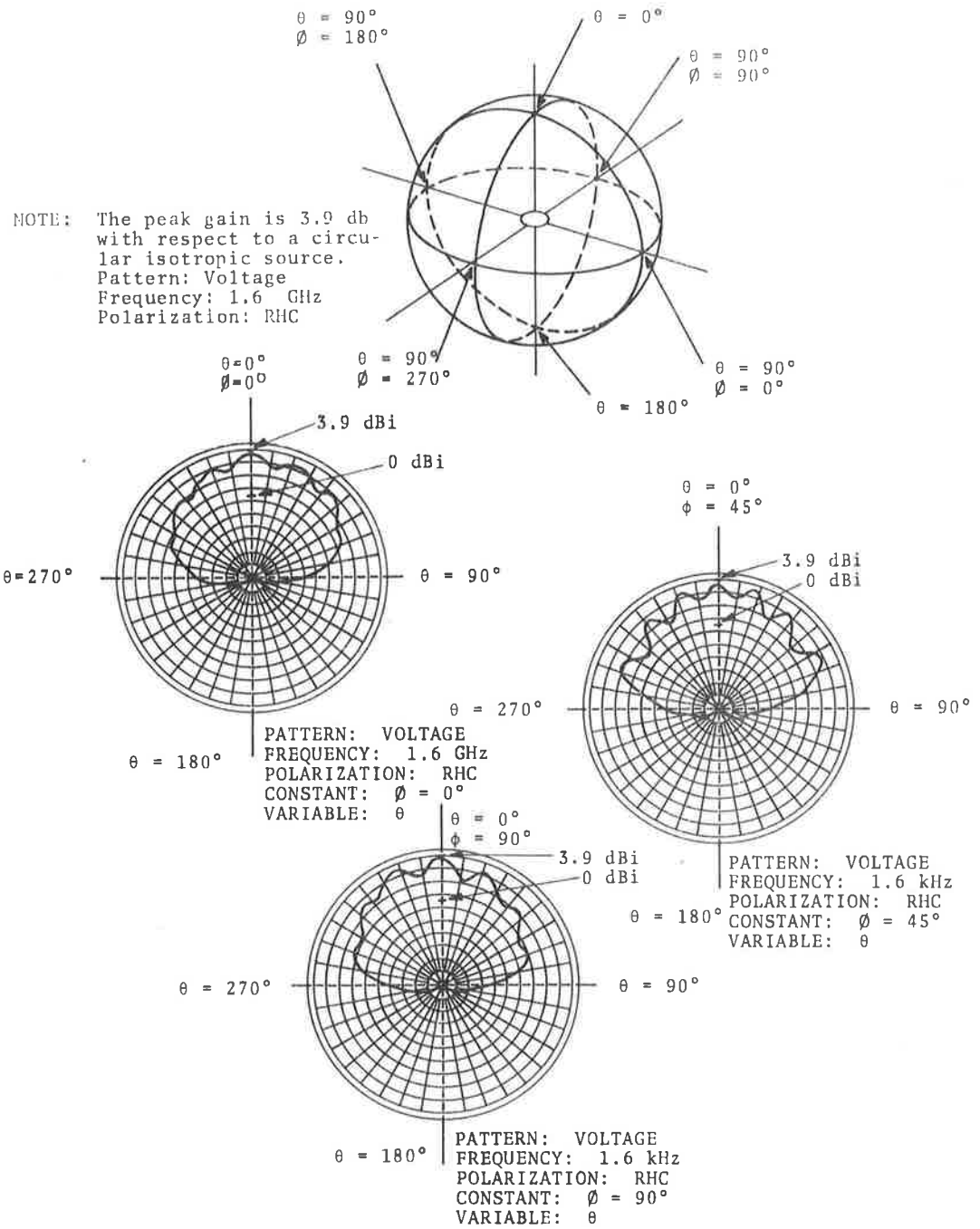
Figure 10.   TRW Curved Turnstile Antenna Patterns

29

The antenna patterns shown in Figure 10 were obtained from measurements of the antenna mounted on a 4 ft. x 6 ft. ground plane with a 5 ft. radius of curvature in the longer dimension. The patterns are plotted in units of voltage.

The peak gain of the antenna is 3.9 dB with respect to a circular isotropic source.

3.4 REFERENCES

1. Applications of Satellites to Communications, Navigation and Surveillance for Aircraft Operating over Contiguous United States. TRW (Technical Proposal to NASA Electronics Research Center, Cambridge, MA, 14671.000). October, 1969.

2. Study of a Navigation and Traffic Control Technique Employing Satellites. Vol. III. TRW Report No. 08710-6014-R000. TRW Systems Group, prepared under NASA Contract NAS-12-539, December 1967.

4. BOEING L-BAND ORTHOGONAL-MODE CAVITY ANTENNA

The orthogonal-mode cavity antenna has a small size, is relatively simple, and provides good low angle coverage associated with its small aperture.

The orthogonal-mode cavity antenna shown in Figure 11 is based on a circular waveguide section with a crossed-slot iris at the end of the waveguide serving as an aperture which provides a low-gain circularly polarized radiator with hemispherical coverage. Orthogonally polarized TE_{11} modes are established in the circular waveguide by two orthogonal dipole feeds excited with equal amplitude. Phase quadrature excitation is used to provide circular polarization at the aperture of the waveguide. The 5.0-inch dimension of the waveguide allows propagation of only one mode. The next higher mode, TM_{01}, requires a diameter of 5.6 inches, and therefore does not propagate.

The antenna radiation pattern coordinate system used for all experimental work is shown in Figure 12. The two-axis model positioner provides the coordinate direction movements indicated by θ and $\emptyset$ on the coordinate system diagram. A polarization positioner provides the capability for changing the electric-field vector polarization from E (θ) to E ($\emptyset$) or any intermediate angle. Continuous rotation of this positioner enables recording of polarization patterns from which the ellipticity ratio can be determined.

The patterns shown in Figures 13 and 14 are for the antenna on top centerline.

    a.   Pitch Plane $\emptyset$ = 0°; θ = variable

    b.   Roll Plane $\emptyset$ = 90°; θ = variable.

Scale model pattern measurements were performed to determine the radiation pattern characteristics of the "orthogonal mode cavity" circularly polarized L-band antenna installed on Boeing 707 airplane at STA 820 top centerline.

31

CROSSED SLOT

MOUNTING FLANGE
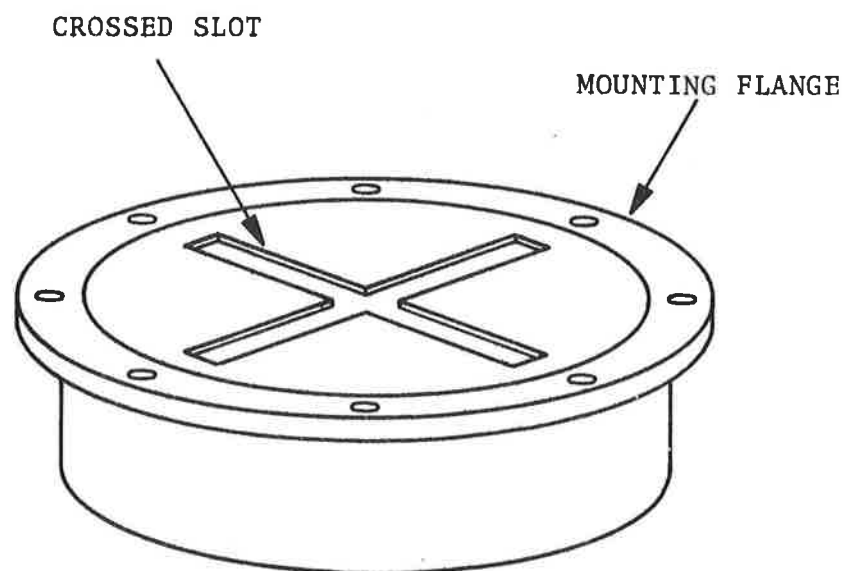
Figure 11. Sketch of L-Band Orthogonal-Mode Cavity Antenna

(a) Coordinate system

(b) Conical patterns
θ constant
ϕ variable

(c) Principal plane patterns
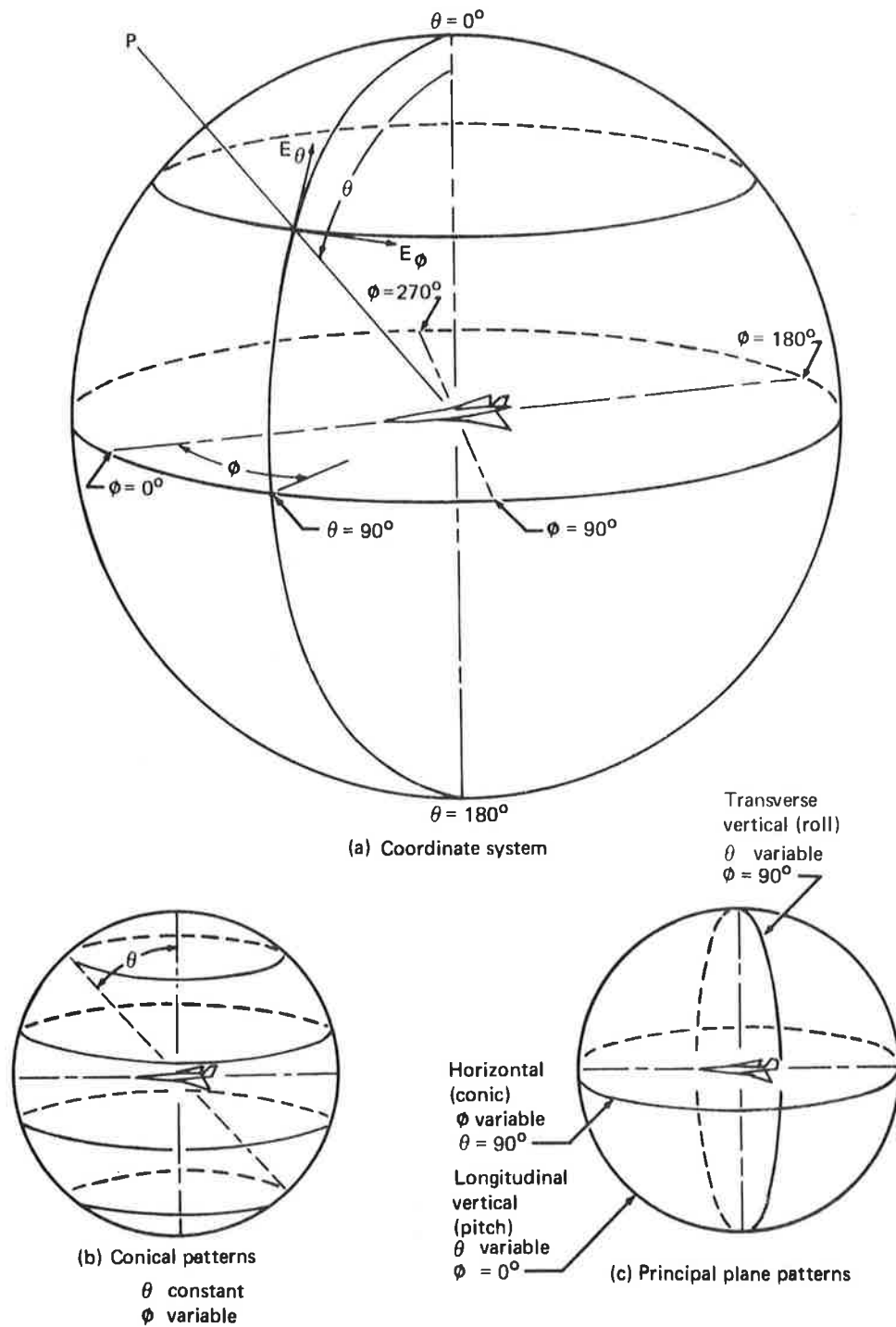
Figure 12. Antenna Range Coordinate System

33

θ 90°

180° 0°

90°

θ=90°

θ=180° θ=0°

θ=90°

Directivity: 5.6 dB
Curve plotted in voltage
Variable angle θ
Constant angle φ=0°

Model scale: 1/20
Scale frequency: 32 GHz
Boeing 707 airplane
Antenna location: top centerline
at STA 820
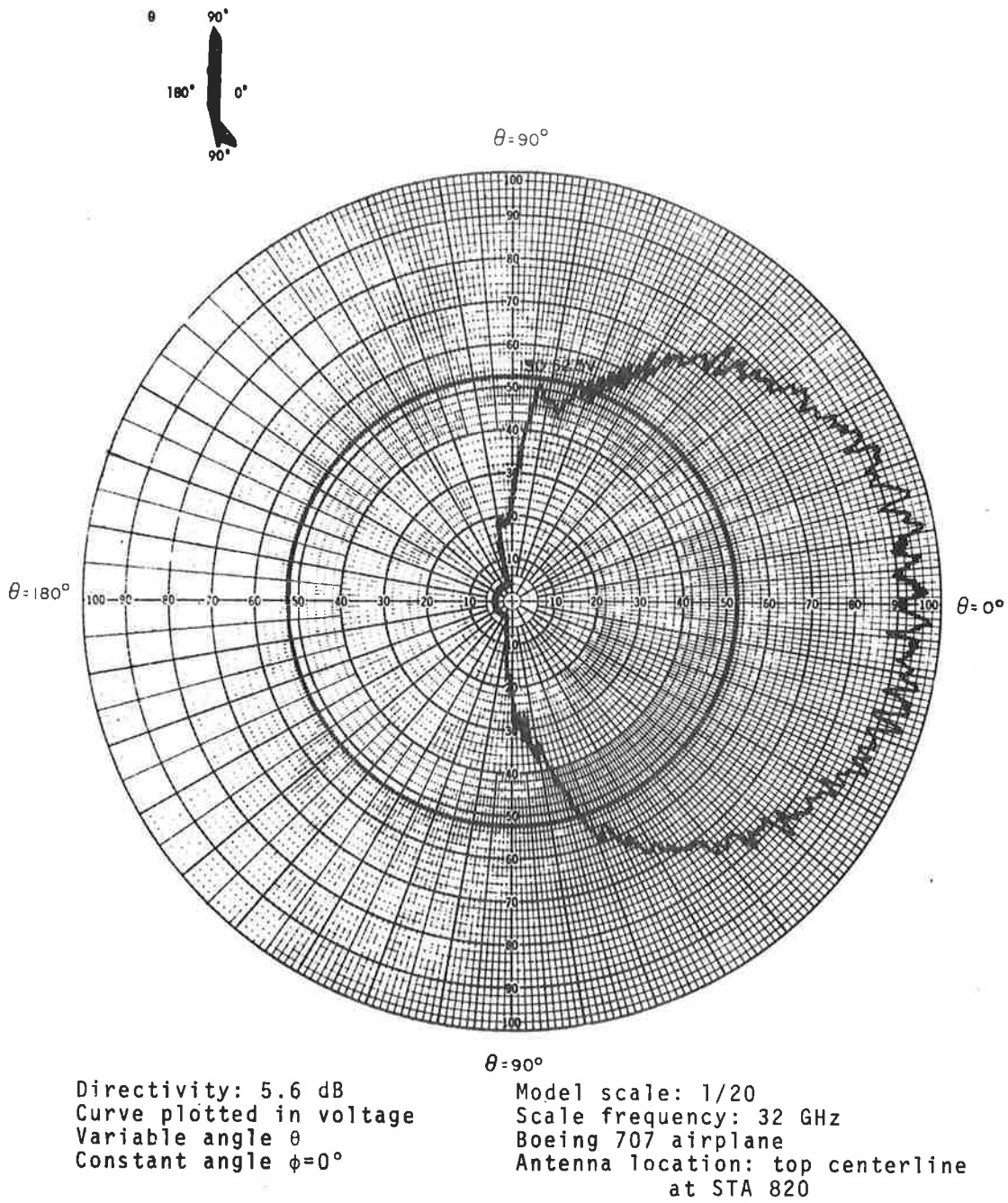
Figure 13.   Orthogonal-Mode Crossed-Slot Antenna Pitch Plane
            Pattern, Right-Hand Circular (Principal) Polarization

34

Directivity: 5.6 dB
Curve plotted in voltage
Variable angle θ
Constant angle φ=90°

Model scale: 1/20
Scale frequency: 32 GHz
Boeing 707 airplane
Antenna location: top centerline
at STA 820

Figure 14.   Orthogonal-Mode Crossed-Slot Antenna Roll Plane
Pattern, Right-Hand Circular (Principal) Polarization
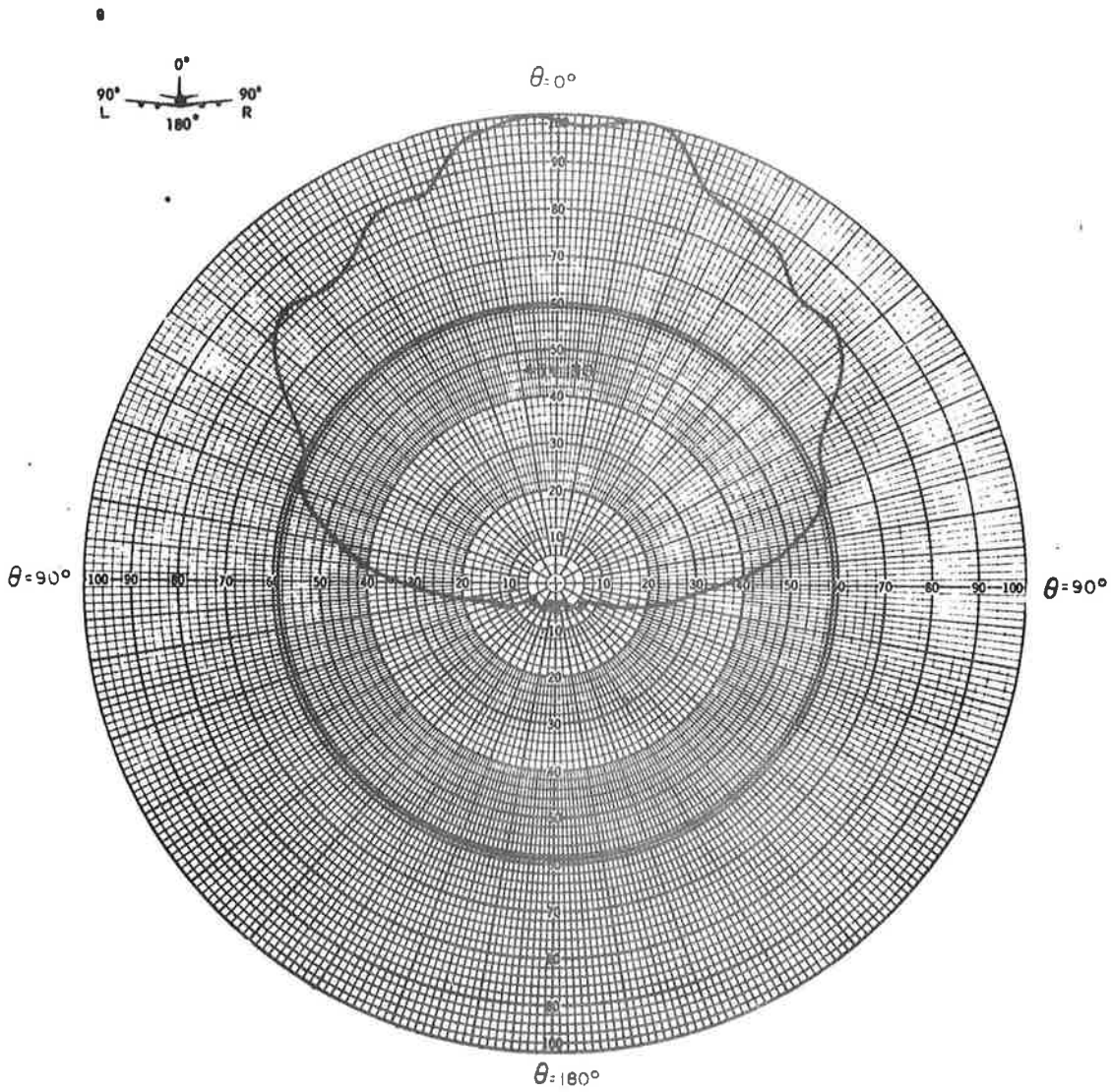
Curve plotted in voltage   Model scale: full
Variable angle θ   Frequency: 1600 MHz
Constant angle φ = 90°   Antenna location: 4' x 4' ground
Polarization Right Hand   plane
         Circular

Figure 15.   Orthogonal-Mode Crossed-Slot Antenna Roll Plane
         Pattern, Left-Hand Circular Polarization

Due to the similarity between the CONVAIR 880 and the BOEING 707 airframe, a 1/20th scale model 707 airplane was used for the measurements. A scale model antenna was fabricated and installed at the equivalent location on the model airplane. As the subject L-band antenna operates at 1540 to 1660 MHz, the frequency used for the scale model pattern measurements was 32 GHz.

4.1 RESULTS

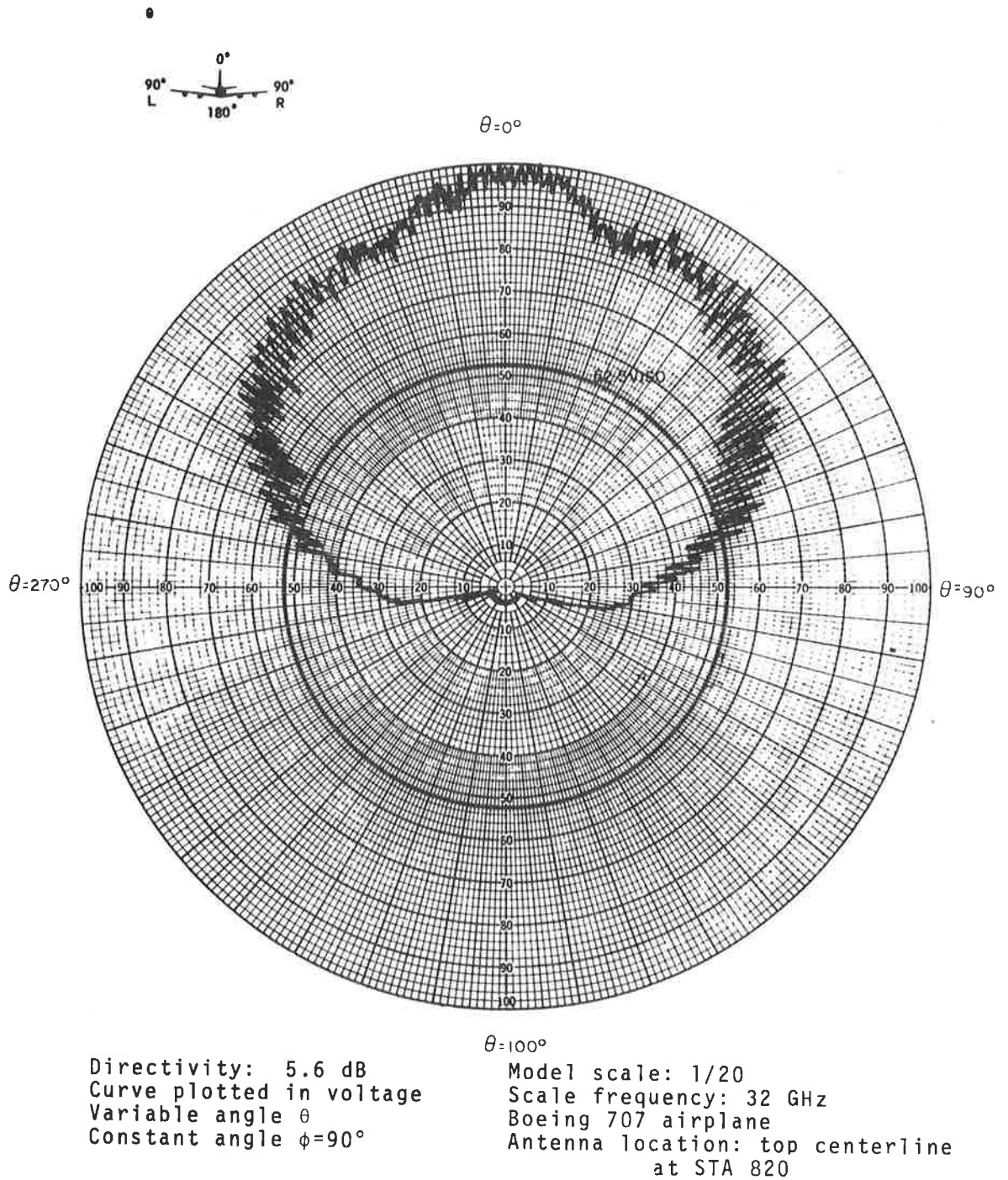### 4.1.1 Polar Diagram Radiation Patterns

These patterns are plotted in voltage with the maximum radiation level referred to the edge of the polar diagram (the "100" level).

The radiation pattern was measured in the following "cuts":

a)   Pitch   (vertical plane through the longitudinal axis)

b)   Roll   (vertical plane normal to the longitudinal axis).

The constant angle, the variable angle, and the polarization of the RF field are indicated on each polar diagram. Patterns are submitted for right-hand circular polarization only.

To demonstrate the accuracy of scale measurements, the model antenna was installed on a 2.4-inch by 2.4-inch curved groundplane and polar diagram radiation patterns in the pitch and roll cuts were measured (at the scaling frequency: 32 GHz).

These patterns were almost identical to those measured on the full scale antenna mounted on a 4-foot by 4-foot groundplane (Figure 15).

4.1.2 Integration

The total energy radiated over the sphere (right-hand polarized as well as left-hand polarized energy) was integrated to establish the directivity of the antenna as installed on the scale model airplane. The directivity of the antenna as installed is 5.6 dB.

For the L-Band antenna installed at 35° to the right of top centerline, the total energy radiated over the sphere (right-hand polarized as well as left-hand polarized energy) was integrated to establish the directivity of the antenna as installed on the scale model airplane. The maximum directivity of the antenna as installed is 7.0 dB.

A pattern is reported for the antenna installed at 35° to the right of top centerline.

Roll Plane $\emptyset$ = 90°; θ = variable.

4.2 REFERENCE

1. L-Band and VHF Hemispherical-Coverage Antennas for Satellite Communication. The Boeing Company (Technical Proposal to DOT Transportation Systems Center, D6-24782). 1970.

5. BOEING FOUR-ARM LOG-SPIRAL ANTENNA

The planar, log-spiral antenna has good coverage but shows no advantage over the orthogonal-mode antenna and does, of course, have the disadvantage of a relatively complex feed and mode-switching network.

The four-arm log-spiral antenna designed by Boeing shown in Figure 16 consists of a planar dielectric sheet supporting four radiating elements. This assembly is mounted over a right-circular cylindrical cavity of about 0.9 wavelength in diameter. The edges of one arm are designed in polar coordinates by the relationships

$$\rho_1 = e^{\alpha\theta}\rho_o$$

and

$$\rho_2 = e^{\alpha(\theta-\delta)}\rho_o$$

The other arms are defined by successive rotation of the above relationships in increments of $\theta = \frac{\pi}{2}$. The defining parameters are shown in Figure 16. The parameters ρ_o and ρ_m refer to the inner, or feed circle radius and the maximum, or terminating radius, respectively. The theory of multimode excitation of log-spiral antennas has been presented by Dyson and Mayes (see reference 3 below). The sequential numbering of the feed terminals and the mode switching circuitry to provide mode 1 and mode 2 excitation are shown in Figure 17. Mode 1 excitation would be utilized to provide coverage for $0° < \theta < 35°$ and mode 2 would be utilized to provide coverage for $35° < \theta < 80°$. Experimental results obtained at Boeing (reference 2) on an L-band test antenna are shown on a composite gain curve (in dB relative to isotropic) for
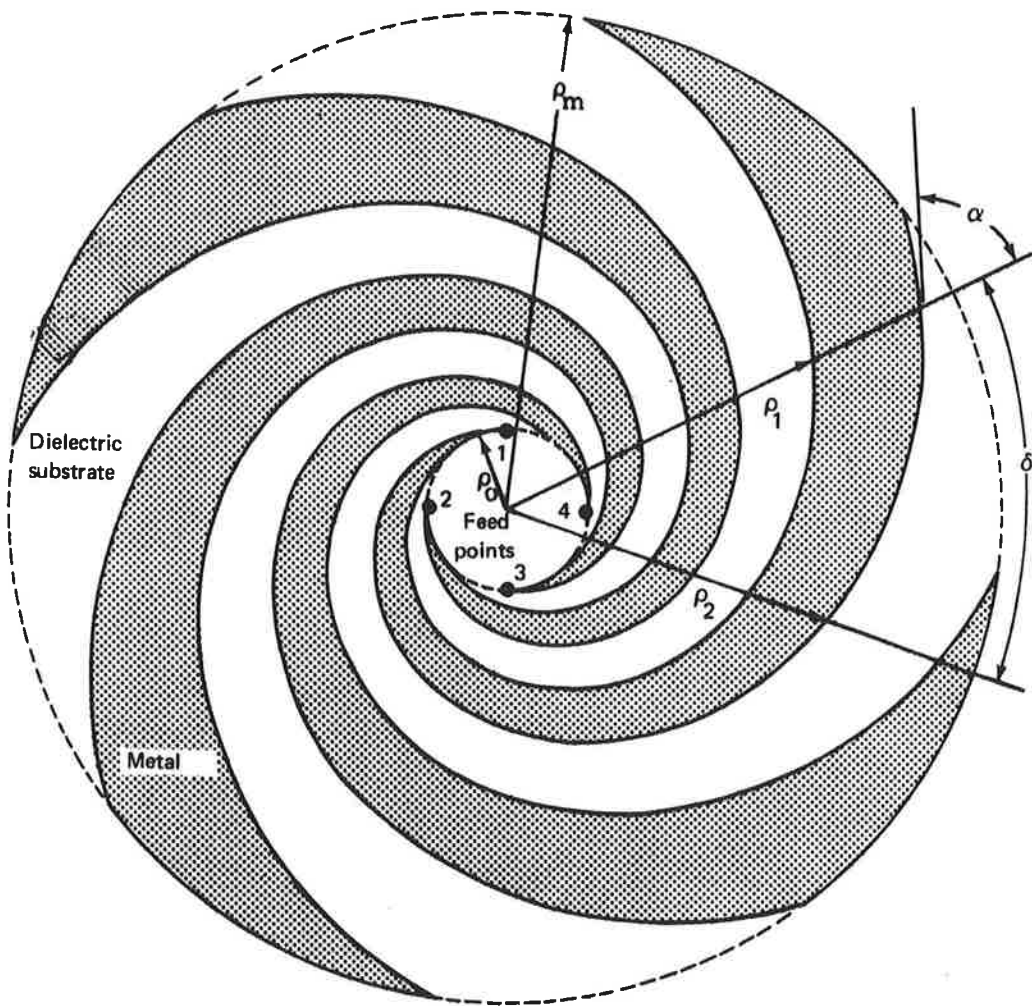
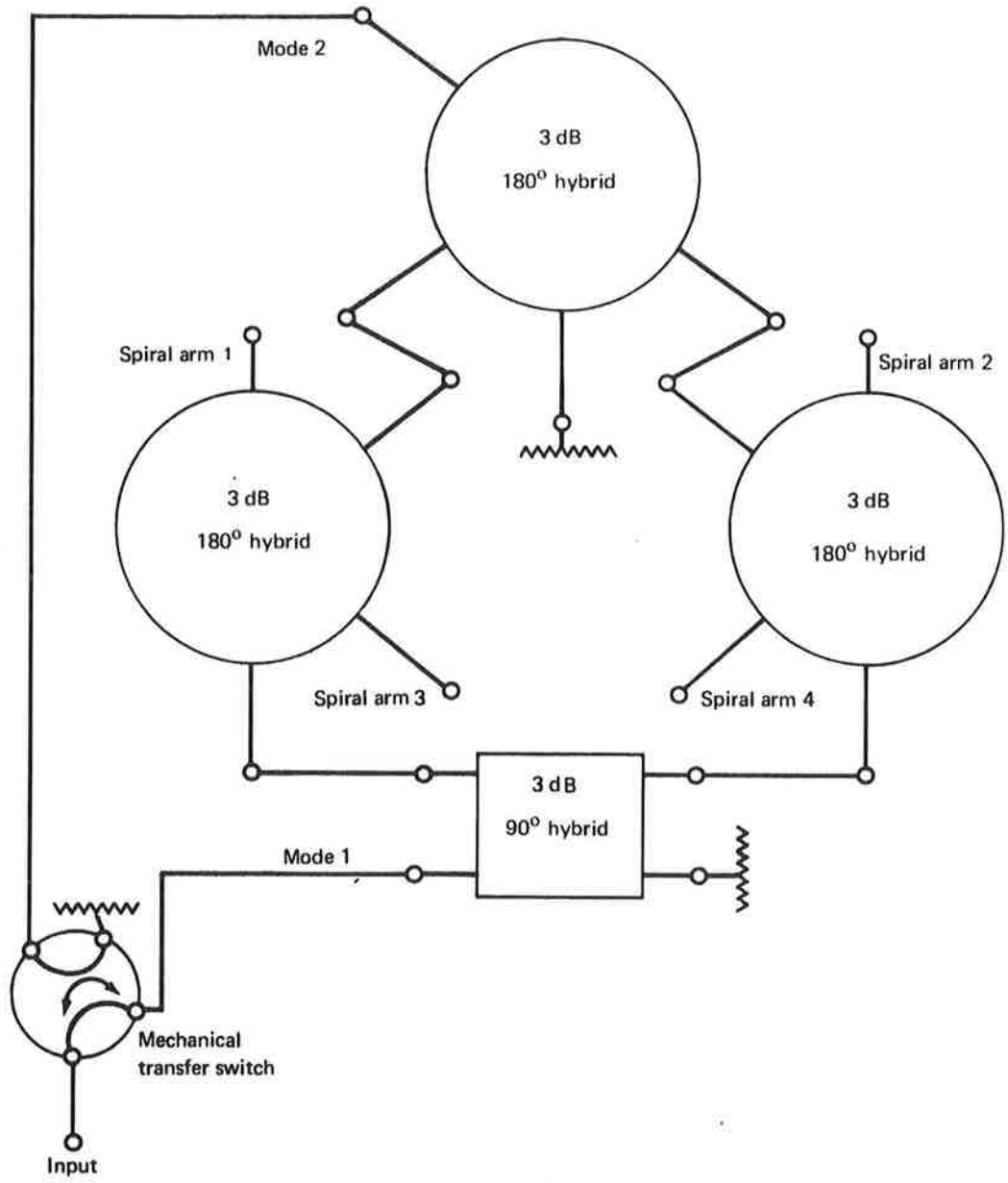Figure 16. Sketch of Four-Arm Planar Log-Spiral

Figure 17. Four-Arm Spiral Mode Switch

41
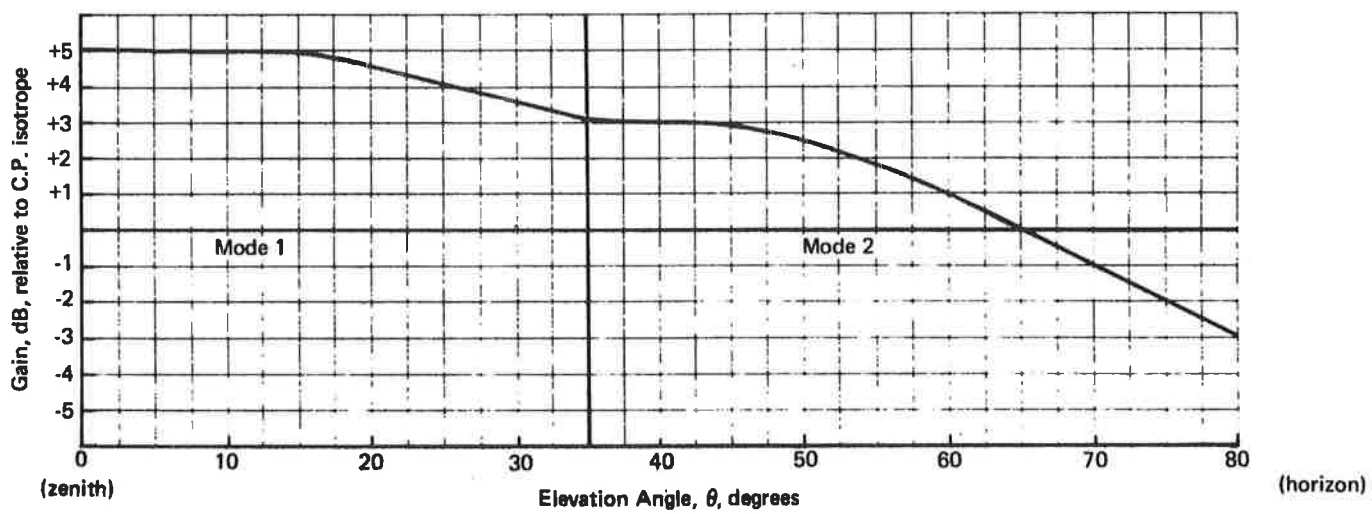
Figure 18. Four-Arm Log-Spiral Antenna Gain

42

modes 1 and 2 versus θ (vertical angle) in Figure 18. The gain
curves shown in Figure 18 include a predicted efficiency value of
64% (-2 dB).

In the past, the log-spiral and other spiral antennas have
been used primarily in receiving and low-power transmitting appli-
cations. This has been due to inherent limitations in dissipating
heat caused by power losses in the elements. However, recent
advances in materials technology have resulted in the development
of low-loss dielectric materials with relatively high thermal
conductivity that can be utilized as the support structure for
spiral elements. This permits the heat generated to be conducted
to the surrounding cavity more readily. For example Transco
has produced UHF (240 to 500 MHz) spiral antenna rated at 2000
watts averaged power input.

5.1 REFERENCES

1. Experimental L-Band SST Satellite Communications/Surveillance
   Terminal Study. Vol. IV, Aircraft Antenna Studies. The
   Boeing Company (Contract NAS 12-621), November 1968.

2. Majeau, H., Antenna Research for Airborne Penetration Aids (U).
   Document D6-23451. The Boeing Company, 1968, Secret.

3. Dyson, J.D., and P.E., Mayes, New Circularly Polarized
   Frequency-Independent Antennas with Conical Beam or Omni-
   directional Patterns. ITE Transactions on Antennas and
   Propagation, Vol. AP9, No. 4, July 1961, pp. 334-342.

4. Anon., 1968 Product Data Sheet 322. Transco Products Inc.,
   4241 Glencoe Ave., Venice, California.

5. Study Report on L/S Band Antenna for 621B Program.
   Appendix I (70-7343.1-50) TRW System Group. May 1970.

6. BOEING SLOT-DIPOLE ANTENNA

The slot-dipole antenna (see Figure 19) incorporates an
actively fed dipole and a parasitic slot. The radiated polar-
ization of the dipole is orthogonal to that of the slot, and the
desired circular polarization results when the two orthogonal
components of radiation are made equal in magnitude with a phase
difference of 90°. This is accomplished by adjusting the im-
pedance of the slot and the angle of the dipole with respect to
the slot. Slot impedance is determined by the slot width, the
dimensions of the cavity, and the shape of any additional para-
sitic elements.

Antenna radiation patterns have been taken for a slot-dipole
L-band antenna system. The antenna system requires three slot-
dipole antennas located around the fuselage periphery. One antenna
is located at top centerline, one at 55 degrees to the left of
top centerline, and one at 55 degrees to the right of top center-
line. Only one antenna will be in use at a time with a coaxial
switch selecting the correct antenna.

The slot-dipole antenna is ideally suited for this type of
installation since it has a narrow roll-plane pattern along with
a wide pitch-plane pattern. Figures 20 and 21 are the principal
plane patterns of a slot-dipole antenna at station 430 on top
centerline of a 707 aircraft. Figure 22 is a roll-plane pattern
of a slot-dipole antenna installed at station 430 and 55 degrees
to the right of top centerline. Radiation distribution plots of
both of these antenna locations are included on Figures 26 and 27.
Both principal polarization circular and cross-polarization cir-
cular are included.

Antenna radiation patterns of the 55 degrees to the left
location were not taken since these patterns are completely sym-
metric with the 55 degrees to the right of top centerline location.

44

DIPOLE ELEMENT

GROUND PLANE

REACTIVE STUB
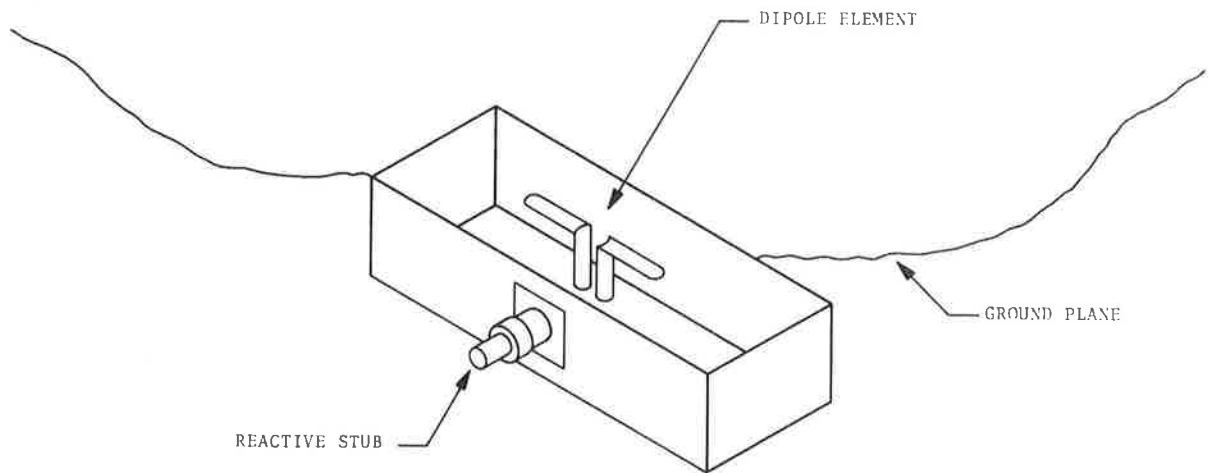
Figure 19. Slot Dipole Antenna
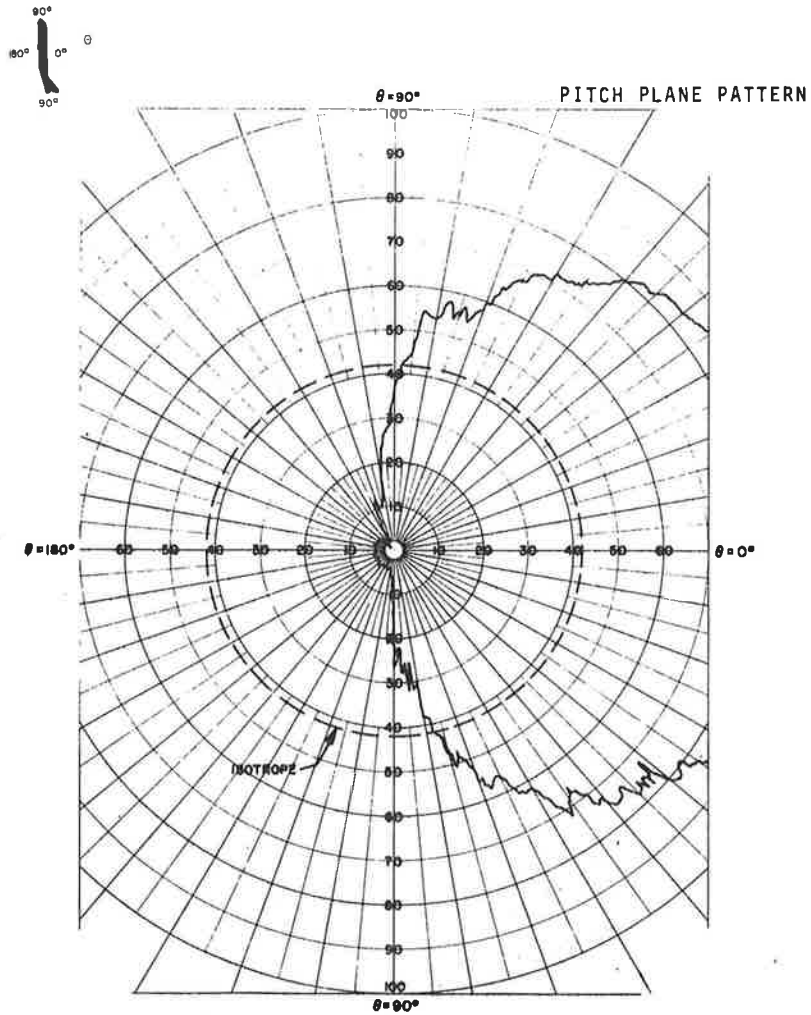
45

PITCH PLANE PATTERN

PLANE TYPE ___707___ MODEL SCALE __1/20__
ANTENNA TYPE_____SLOT DIPOLE
ANTENNA LOCATION _STA 430 TOP CENTERLINE_
FULL SCALE FREQUENCY ___1540 MHZ___

PEAK GAIN = 7.5 db

VARIABLE ANGLE θ (✓)
CONSTANT ANGLE φ:_0____
POLARIZATION RIGHT HAND CIRCULAR

Figure 20. Principal Pitch Plane Pattern (A)
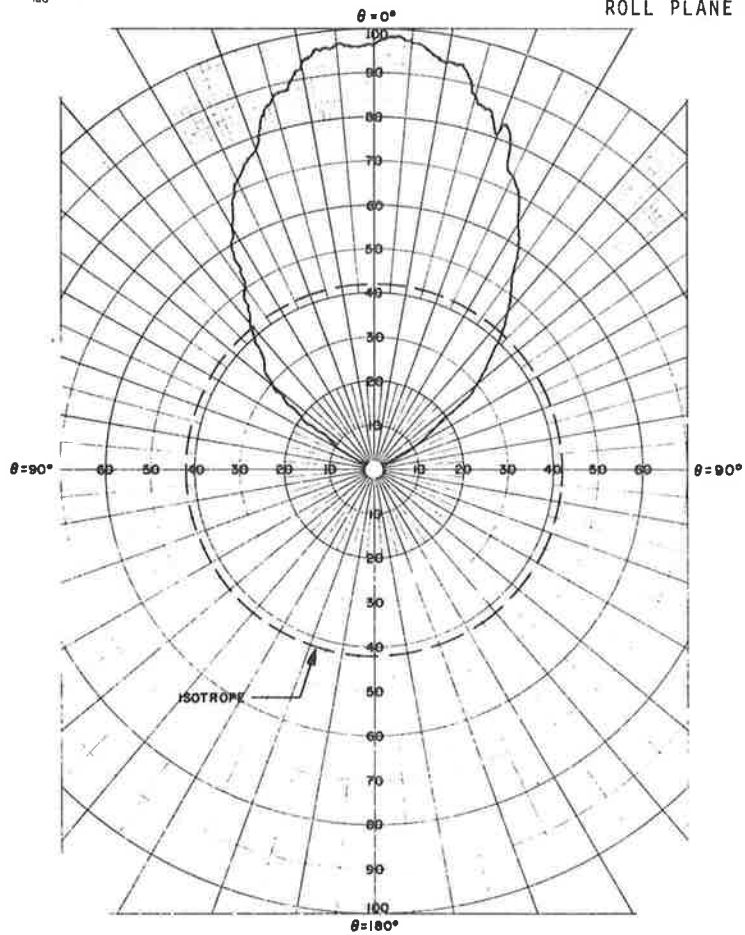
46

PLANE TYPE _____ 707 _____ MODEL SCALE _1/20____
ANTENNA TYPE ____ SLOT DIPOLE _____
ANTENNA LOCATION _ STA 430 TOP CENTERLINE _____
FULL SCALE FREQUENCY _____ 1540 MHZ _____

PEAK GAIN = 7.5 db

VARIABLE ANGLE θ (✓)
CONSTANT ANGLE φ: _90____
POLARIZATION RIGHT HAND CIRCULAR

Figure 21.   Principal Roll Plane Pattern (B)
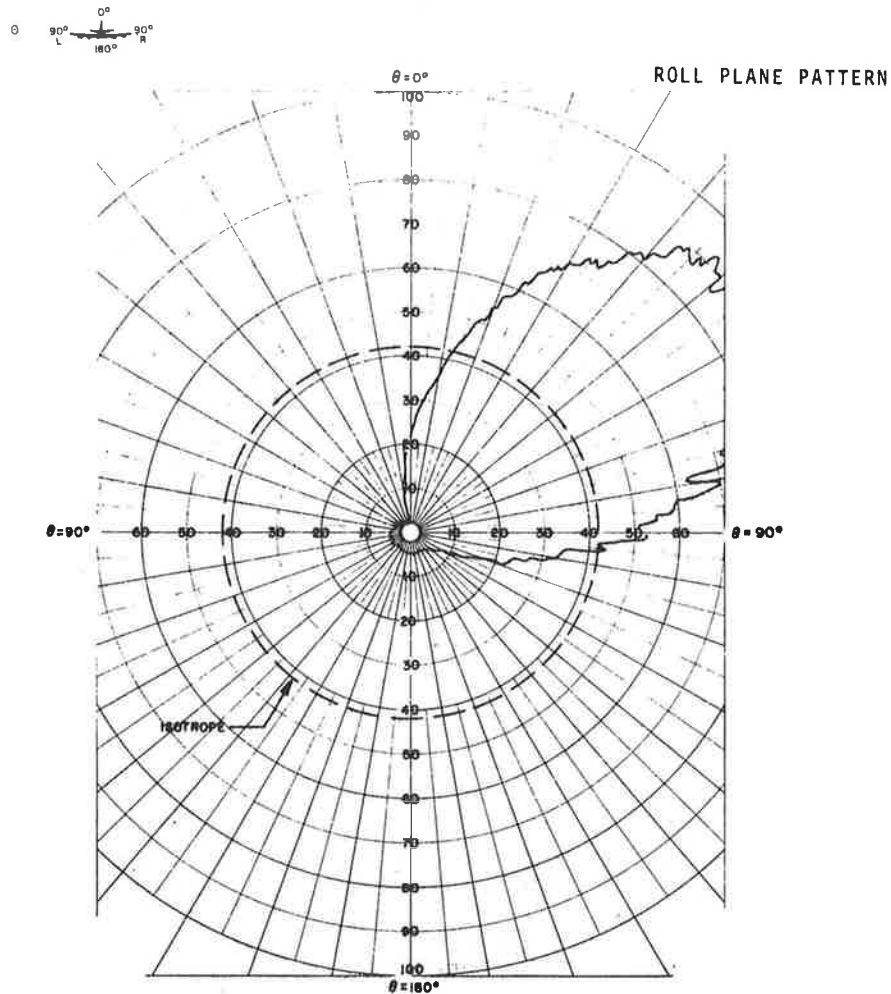
47

Figure 22. Principal Roll Plane Pattern (C)

The peak antenna gain at each antenna location is 7.5 dB with respect to a circular isotrope. This gain figure assumes a 0.5-dB antenna loss. The pattern maximum on the top centerline location radiation plot is two; therefore, two represents a peak gain of 7.5 dB. The pattern maximum at 55 degrees to the right of top centerline location is three; therefore, three represents the peak gain of 7.5 dB for the side-mounted slot-dipole antenna location. Knowing these data, the antenna with the highest gain in any given direction will be the one selected.

Figures 23 through 26 represent conics of two slot-dipole antenna installations. Figures 23 and 24 are conic patterns for a three-antenna configuration: one antenna at top centerline, one at 55 degrees to the right of top centerline, and one at 55 degrees to the left of top centerline. The patterns are the response of the antenna to right-hand circular polarization. To avoid confusion from pattern overlap only half-conics are taken since the conics are completely symmetric about the fore-aft axis. Conics are shown from θ = 10 degrees to θ = 110 degrees. These patterns were taken at body station 500 on a 1/7th scale 707 aircraft model.

The numbers labeled dB ranging from 0 through 10 represent the radius of constant gain circles. These patterns are composite patterns with the antenna of the highest gain chosen in any particular direction. In operation only one slot dipole is in use at a time with a coaxial switch selecting the correct antenna.

Figures 25 and 26 represent a family of conics for a two slot-dipole antenna installation. One antenna is located at 35 degrees to the right of top centerline and the other at 35 degrees to the left of top centerline at body station 1135. Only one antenna is in use at a time with the antenna providing the highest gain being the one selected. This antenna system provides somewhat lower gain over the intended coverage sector, i.e. θ = 0 to θ = 80 degrees, than the three-antenna configuration. These patterns are also recorded as half-conics and are the response of the antenna to right-hand circular illumination.
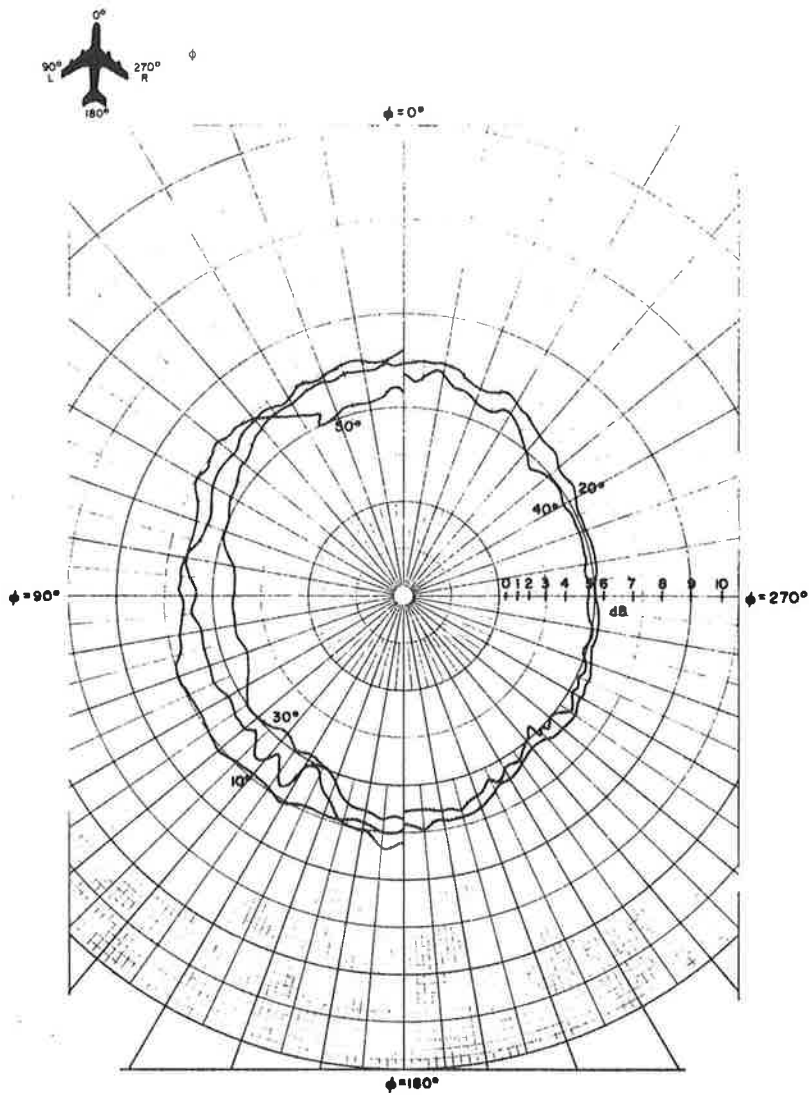
PLANE TYPE__707_____ MODEL SCALE__1/7____
ANTENNA TYPE__SLOT DIPOLE_____
ANTENNA LOCATION_STA 500-TOP C/L - 55° OFF TOP
FREQUENCY FULL SCALE_____ MODEL_`C/L_____

VARIABLE ANGLE φ (√) θ (10, 20, 30, 40, 50)
POLARIZATION   RIGHT HAND CIRCULAR
φ=Horizontal angle θ=Vertical angle
CURVE PLOTTED IN: DECIBELS (√)

Figure 23.   Conic Patterns, Constant Angle 10, 20, 30, 40, and
             50 degrees
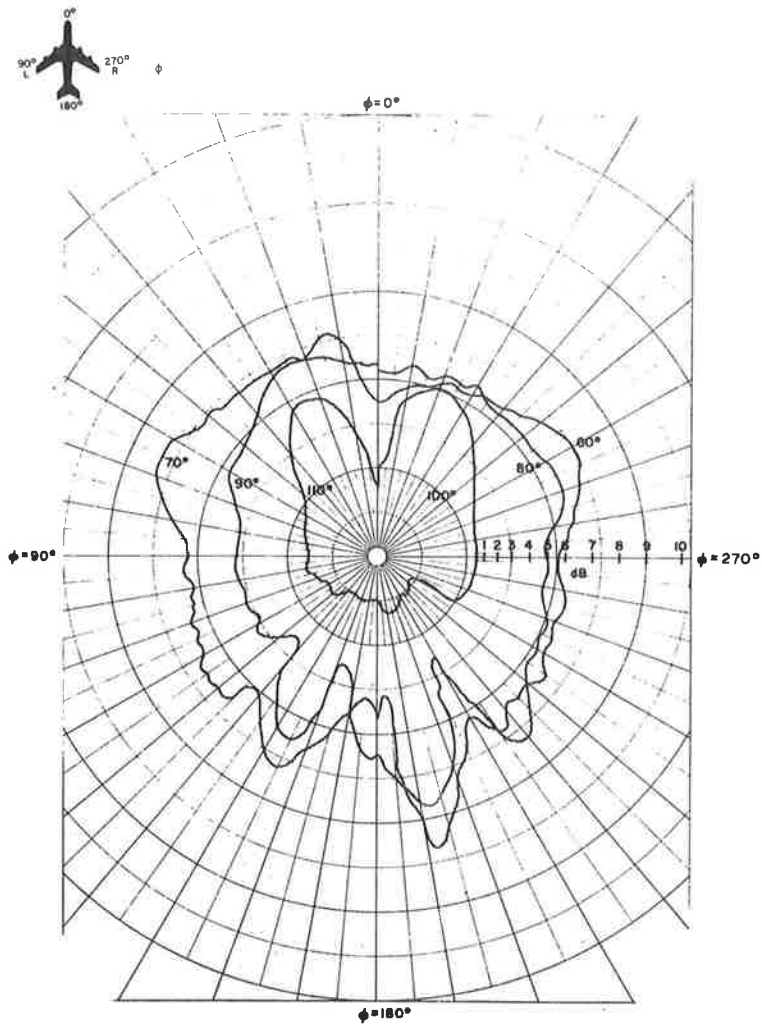
50

PLANE TYPE 707   MODEL SCALE 1/7
ANTENNA TYPE SLOT DIPOLE
ANTENNA LOCATION STA 500-TOP C/L-55° OFF TOP
FREQUENCY FULL SCALE

VARIABLE ANGLE φ (✓) θ ( )
CONSTANT ANGLE φ:____ θ: 60, 70, 80, 90, 100, 110
POLARIZATION RIGHT HAND CIRCULAR
CURVE PLOTTED IN: DECIBELS (✓)

Figure 24.   Conic Patterns, Constant Angle 60, 70, 80, 90, 100,
             and 110 degrees
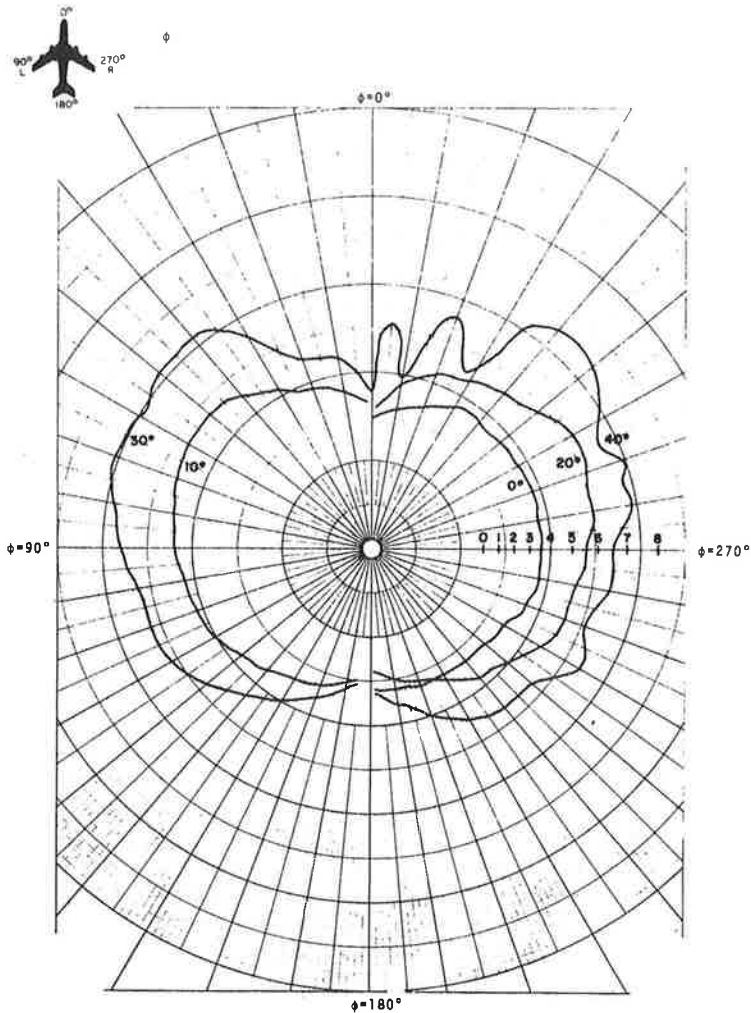
PLANE TYPE_____707_____MODEL SCALE__1/7____
ANTENNA TYPE_____Slot Dipole_____
ANTENNA LOCATION__STA 1135_____
FREQUENCY FULL SCALE_____

VARIABLE ANGLE   φ (✓) θ ( )
CONSTANT ANGLE   φ:_____ θ: 0, 10, 20, 30, 40
POLARIZATION RIGHT HAND CIRCULAR

CURVE PLOTTED IN: DECIBELS (✓)

Figure 25.   Conic Patterns, Constant Angle 0, 10, 20, 30, and
             40 degrees
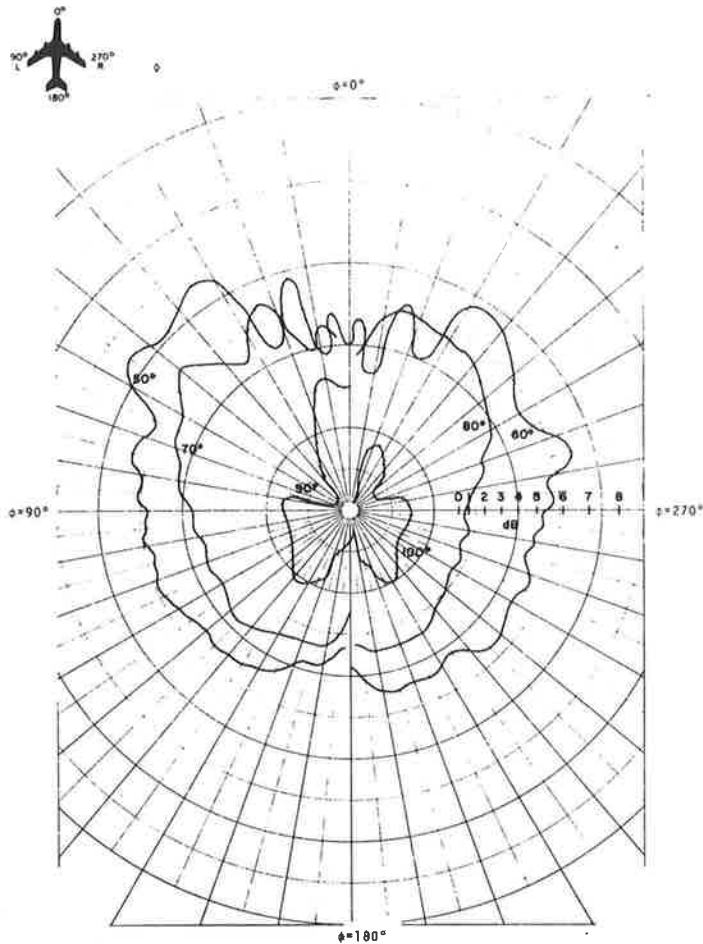
PLANE TYPE____707_____MODEL SCALE_1/7__
ANTENNA TYPE____SLOT DIPOLE_____
ANTENNA LOCATION___STA 1135_____
FREQUENCY FULL SCALE_____

VARIABLE ANGLE φ (✓): φ ( )
CONSTANT ANGLE φ:____ θ: 60, 70, 90, 100, 50
POLARIZATION RIGHT HAND CIRCULAR

CURVE PLOTTED IN VOLTAGE ( ): POWER ( ) DECIBELS (✓)

Figure 26. Conic Patterns, Constant Angle 50, 60, 70, 90, and
100 degrees

The L-band orthogonal slot antenna has been installed at two locations on a simulated Convair 880 aircraft. These two locations are at top centerline and at 35 degrees to the right of top center-line; both locations are at body station 820.

The orthogonal slot antenna is intended to serve as an upper-hemisphere coverage antenna. From the radiation patterns at the top centerline location it certainly accomplishes this by providing an antenna directivity equal to or better than isotropic for a very high percentage of the intended sector coverage, i.e., $\theta = 0$ to $\theta = 80$ degrees. In addition, the coverage below the horizon decreases rapidly below the 100-degree conic. This condition is highly desirable to prevent sea-reflected signals from entering the receiver.

The radiation patterns at 35 degrees off top centerline show the influence of reflections. The roll pattern indicates lobing due to reflections from aircraft surfaces, namely, the right wing. This antenna is intended to have low gain and wide beamwidth. The wide beamwidth accounts for illumination of aircraft surfaces which in turn cause reflections as evidenced by lobing in the patterns. This antenna cannot be recommended for installation other than top centerline. No significant pattern improvement aft is anticipated by moving the top center line antenna location either fore or aft.

7. BOEING DUAL-MODE LINEAR ANTENNA

The antenna consists of a single cavity with a crossed slot iris. Two output connectors labeled "H" and "V" are located on the bottom of strip transmission line. Thus the antenna consists of two independent slot radiators perpendicular to one another. This antenna is linearly polarized yielding two orthogonal linearly polarized outputs and is not intended to be used as a circularly polarized radiator. Note that the polarization is designated as either $E\emptyset$ or $E\theta$ (Linear Polarization); the antenna coordinate system is shown in Figure 27.

Figure 28 is a sketch of the antenna installed at the center of a four-foot-square ground plane which is curved with a radius of curvature of 71 inches in one plane. Figures 29 through 36 are full-scale patterns. Note that the peak gain of one slot is 4.8 dB while the peak gain of the other slot is 4.0 dB. This difference is attributed to the fact that the ground plane is curved in one plane and not the other.

These patterns do not show any influence of the aircraft structure since they are full-scale patterns of the antenna installed on a small ground plane. The scalloping in the E-plane cuts of Figures 29 and 33 is caused by the finite size of the ground plane (edge effect). The amplitude of the scalloping is slightly less in Figure 33 than 29 due to the curvature of the ground plane in Figure 33 (less edge effect due to the curvature of the ground plane).

7.1 REFERENCE

1. L-Band and VHF Hemispherical-Coverage Antenna for Satellite Communication. The Boeing Company (Technical Proposal to the Transportation Systems Center. D6-24782). 1970.

θ=0°

P

E_θ

θ

E_ϕ

ϕ=270°

ϕ=180°

ϕ=0°

ϕ

θ=90°

ϕ=90°

(a) COORDINATE SYSTEM

θ

(b) CONICAL PATTERNS

θ CONSTANT
ϕ VARIABLE

TRANSVERSE
VERTICAL (ROLL)
θ VARIABLE
ϕ = 90°

HORIZONTAL
(CONIC)
ϕ VARIABLE
θ = 90°

(c) PRINCIPAL PLANE PATTERNS

LONGITUDINAL
VERTICAL
(PITCH)
θ VARIABLE
ϕ = 0°
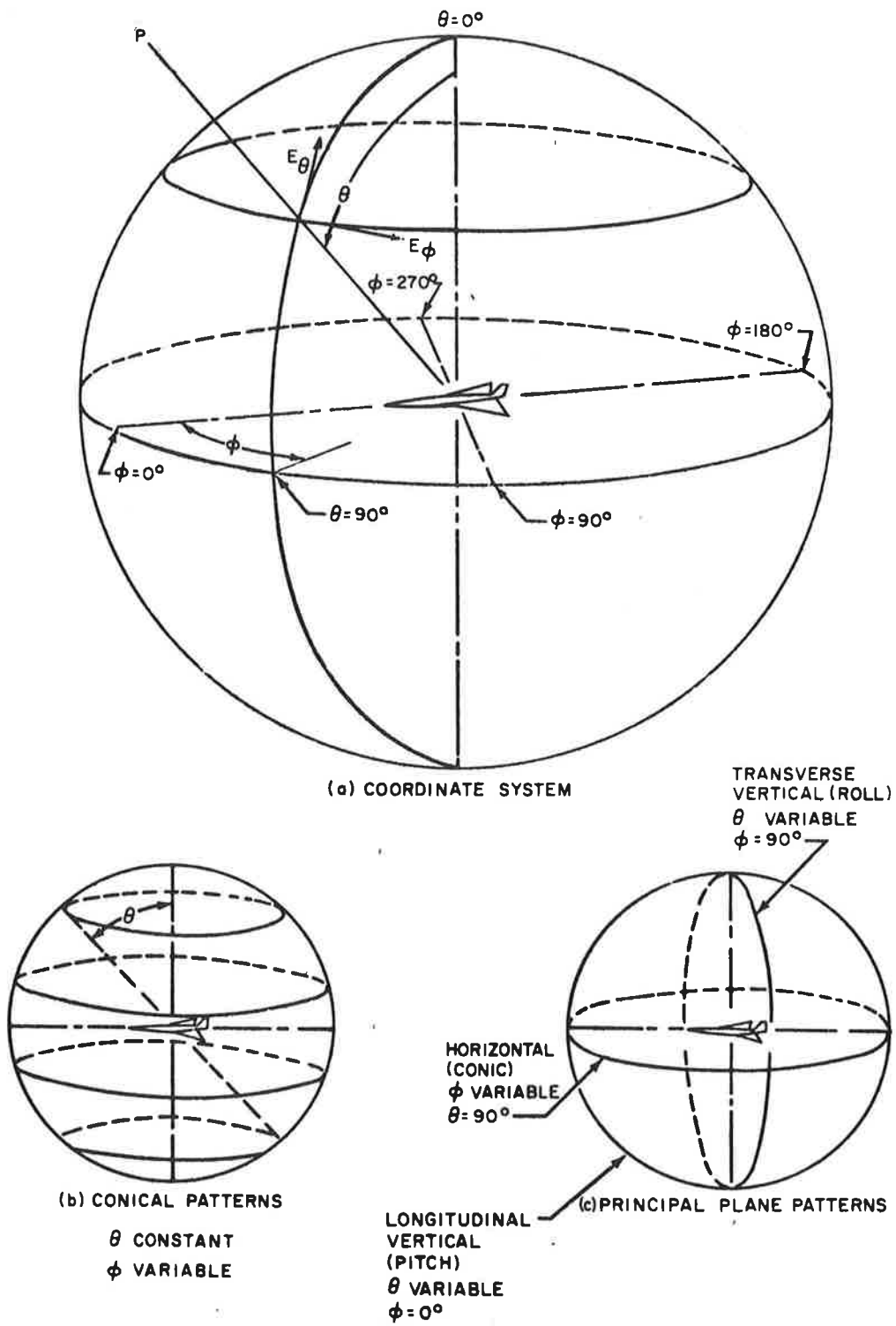
Figure 27.   Antenna Range Coordinate System

LEFT

FORE

4 FT

"V" SLOT — —"H" SLOT

4 FT

AFT

R=71"

RIGHT
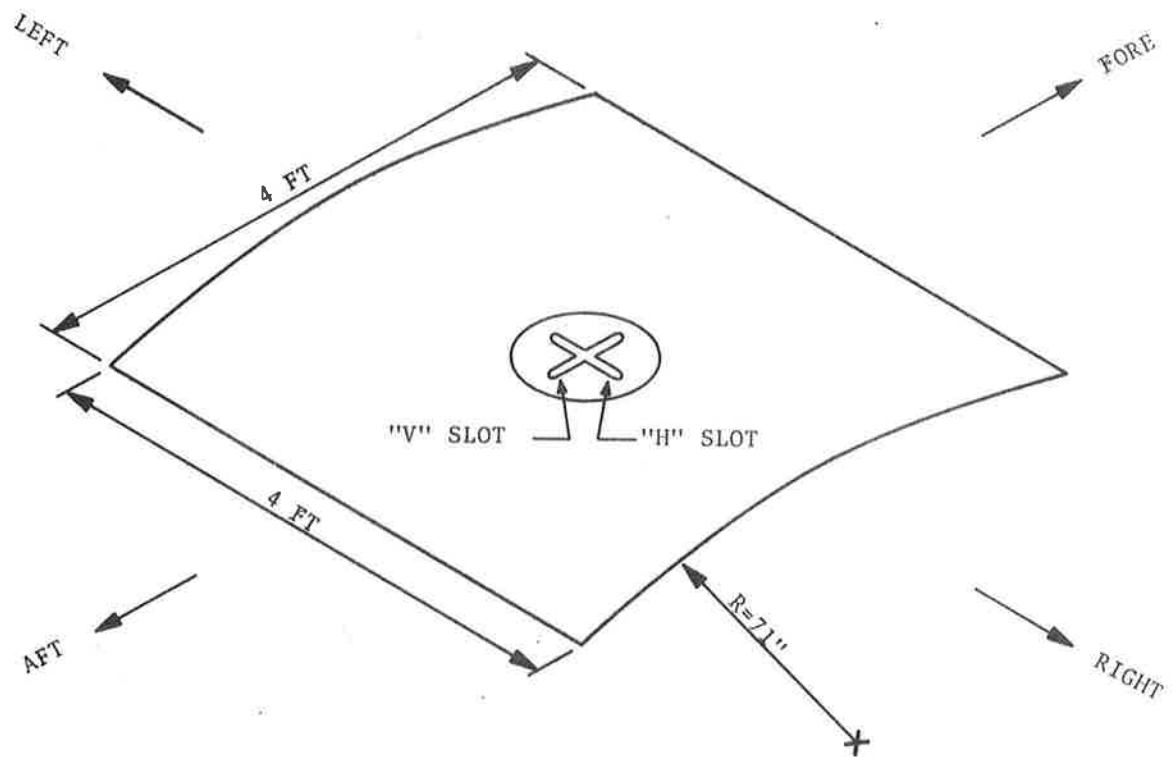
Figure 28. Antenna Installation in Curved Ground Plane
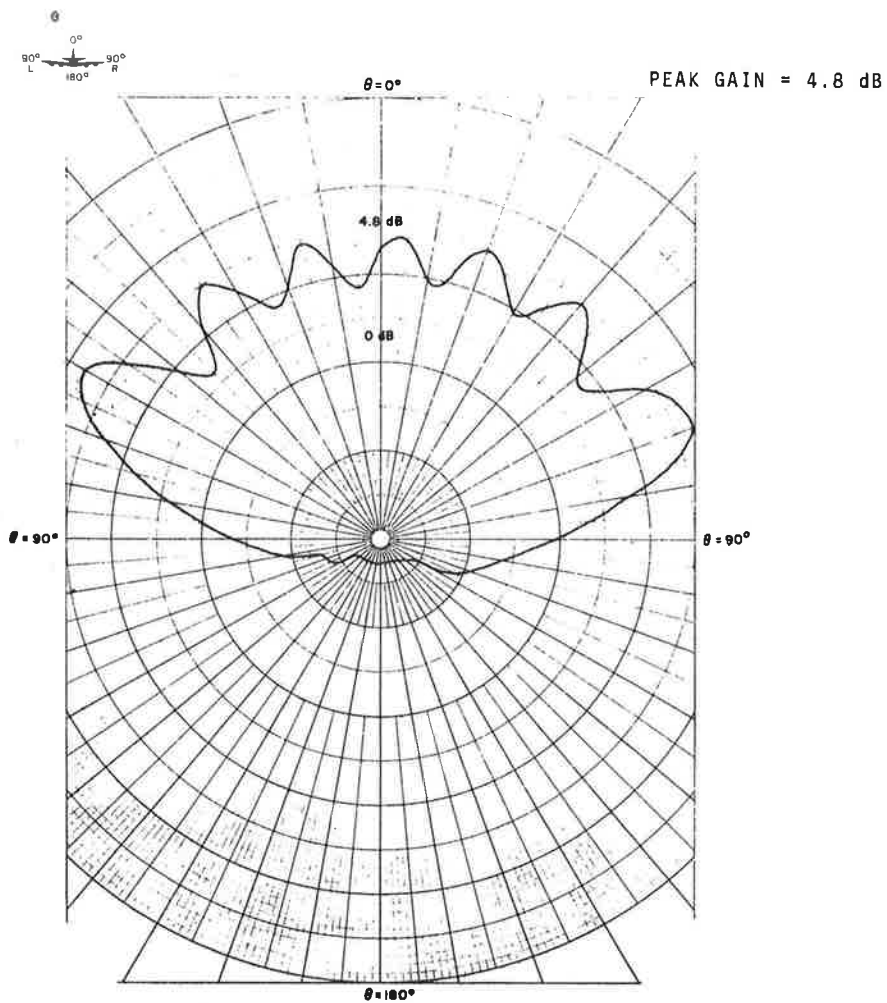
PEAK GAIN = 4.8 dB

θ=0°

4.8 dB

0 dB

θ = 90°   θ = 90°

θ = 180°

PLANE TYPE_____MODEL SCALE FULL
ANTENNA TYPE ORTHOGONAL MODE CAVITY
ANTENNA LOCATION 4 FOOT SQUARE GROUND PLANE
FULL SCALE FREQUENCY 1600 MHZ

"V" PORT
E PLANE CUT

VARIABLE ANGLE φ( ), θ(✓)
CONSTANT ANGLE   φ = 90
POLARIZATION Eφ( ), Eθ(✓)____
CURVE PLOTTED IN VOLTAGE

Figure 29.   Full-Scale Antenna Pattern "V" Port E-Plane Cut

Figure 30. Full-Scale Antenna Pattern "V" Port E-Plane Cut Cross-Polarized

PLANE TYPE_____ MODEL SCALE FULL_____
ANTENNA TYPE ORTHOGONAL MODE CAVITY_____
ANTENNA LOCATION 4 FOOT SQUARE GROUND PLANE
FULL SCALE FREQUENCY 1600 MHZ

VARIABLE ANGLE φ( ),θ(✓)
CONSTANT ANGLE   φ=0 θ=___
POLARIZATION Eφ(✓),Eθ( )___
CURVE PLOTTED IN VOLTAGE

Figure 31.   Full-Scale Antenna Pattern   "V" Port H-Plane Cut
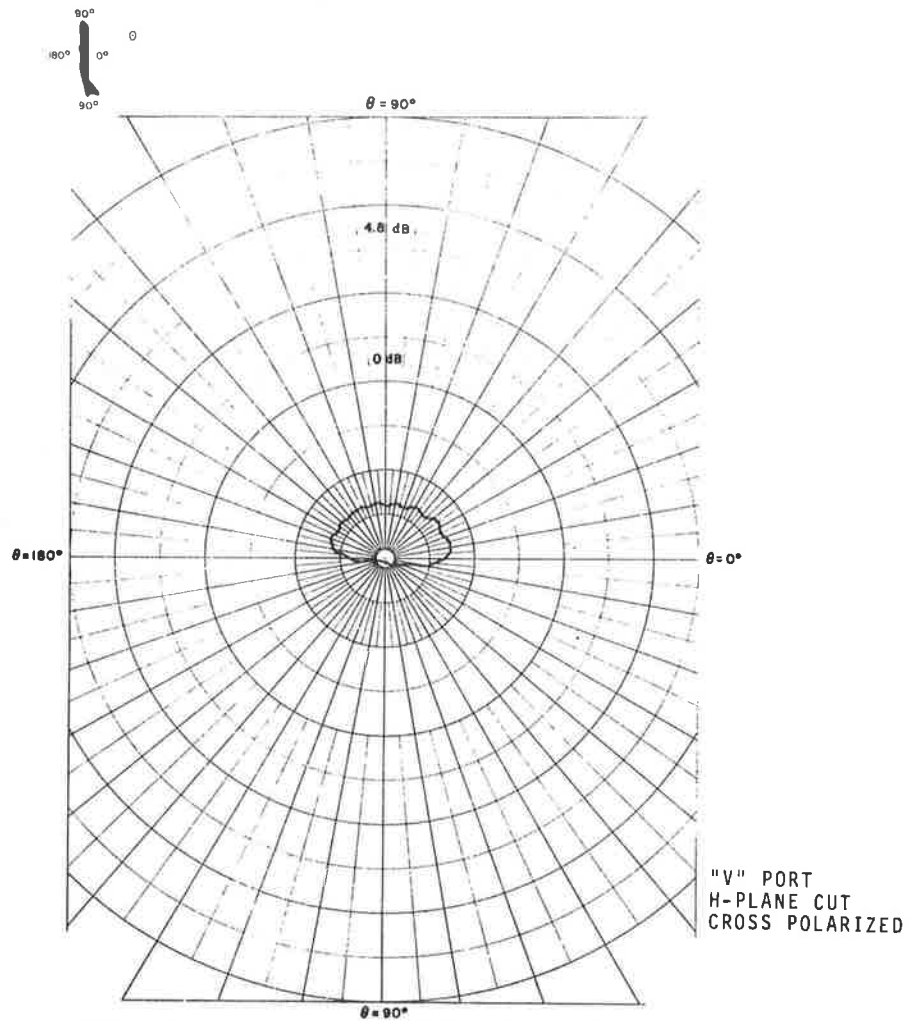
60

PLANE TYPE_____ MODEL SCALE___FULL___
ANTENNA TYPE__ORTHOGONAL MODE CAVITY___
ANTENNA LOCATION_4 FOOT SQUARE GROUND PLANE___
FULL SCALE FREQUENCY___1600 MHZ___

VARIABLE ANGLE Φ( ) θ(✓)
CONSTANT ANGLE Φ:__0_θ:____
POLARIZATION E$_\phi$( ). E$_\theta$(✓)
CURVE PLOTTED IN VOLTAGE

Figure 32. Full-Scale Antenna Pattern "V" Port H-Plane Cut Cross-Polarized

PLANE TYPE_____MODEL SCALE__FULL_____
ANTENNA TYPE ORTHOGONAL MODE CAVITY_____
ANTENNA LOCATION 4 FOOT SQUARE GROUND PLANE
FULL SCALE FREQUENCY___1600 MHZ_____

VARIABLE ANGLE φ ( ): θ (✓)
CONSTANT ANGLE φ 0   θ̄_____
POLARIZATION E$_φ$( ). E$_θ$(✓)
CURVE PLOTTED IN VOLTAGE
PEAK GAIN = 4.0 dB

Figure 33.   Full-Scale Antenna Pattern "H" Port E-Plane Cut
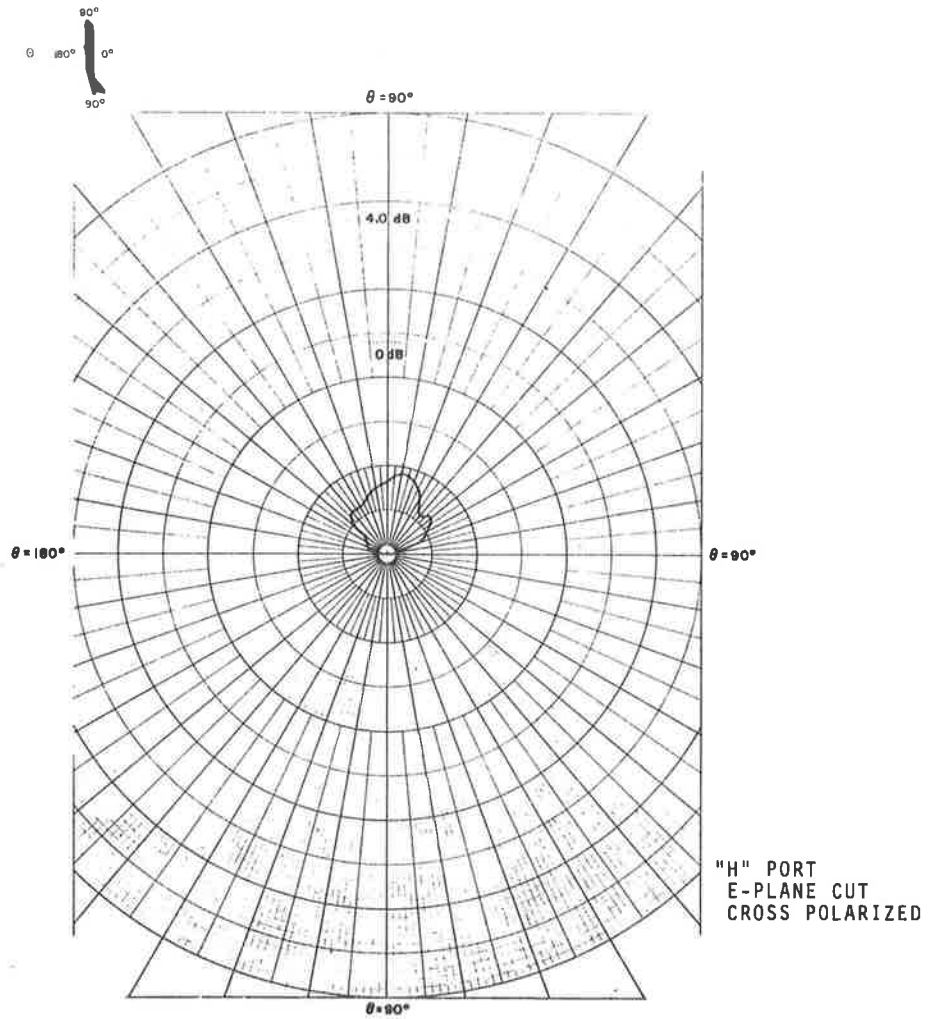
62

θ = 90°

4.0 dB

0 dB

θ = 180°   θ = 90°

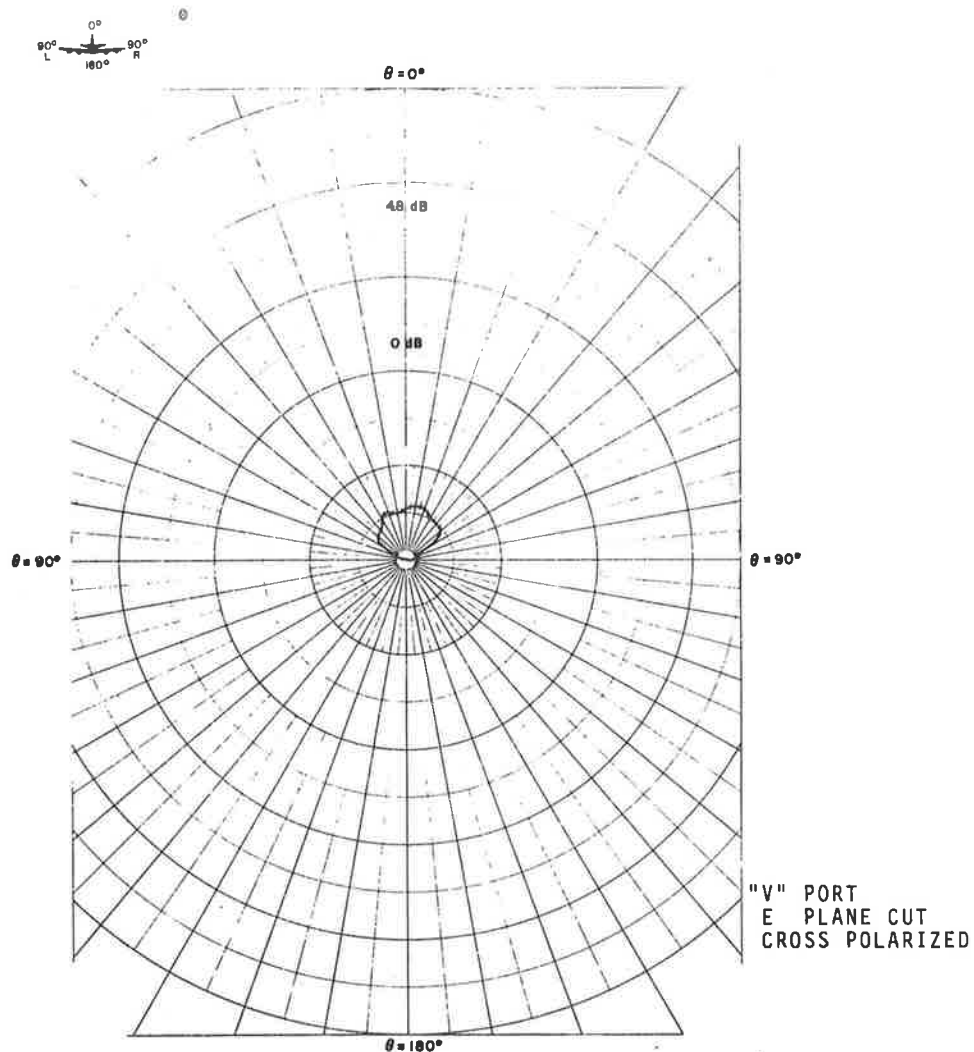θ = 90°

"H" PORT
E-PLANE CUT
CROSS POLARIZED

PLANE TYPE_____ MODEL SCALE FULL_____
ANTENNA TYPE ORTHOGONAL-MODE CAVITY_____
ANTENNA LOCATION 4 FOOT SQUARE GROUND PLANE
FULL SCALE FREQUENCY 1600 MHZ_____

VARIABLE ANGLE φ ( ): θ (✓)
CONSTANT ANGLE φ 0   θ
POLARIZATION   E_φ
CURVE PLOTTED IN VOLTAGE

Figure 34.   Full-Scale Antenna Pattern "H" Port E-Plane Cut
             Cross-Polarized

63

θ = 0°

4.0 dB

0 dB

θ = 90°   θ = 90°

"H" PORT
H-PLANE CUT

θ = 180°
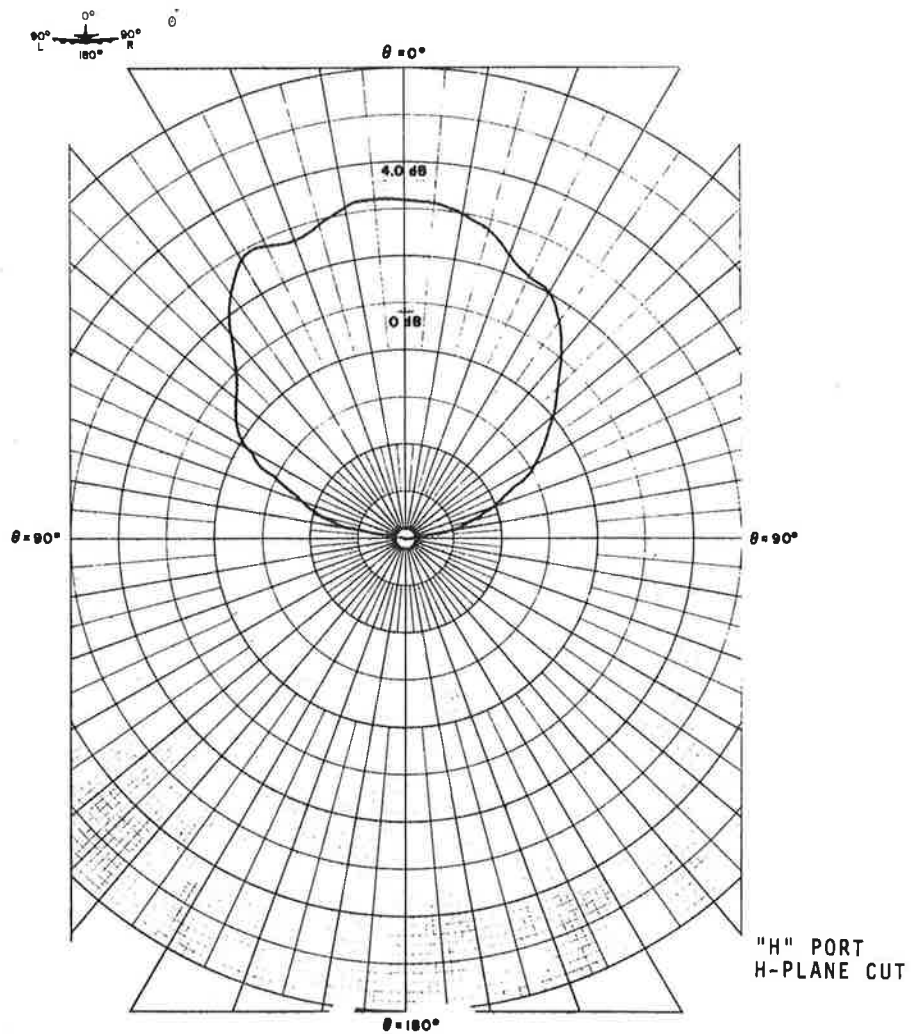
PLANE TYPE_____

ANTENNA TYPE__ORTHOGONAL-MODE CAVITY_____

ANTENNA LOCATION 4 FOOT SQUARE GROUND PLANE

FULL SCALE FREQUENCY 1600 MHZ_____

VARIABLE ANGLE___ϕ (✓): θ (✓)_____

CONSTANT ANGLE   ϕ: _90_ θ: _____

POLARIZATION E_ϕ (✓): E_θ( )_____

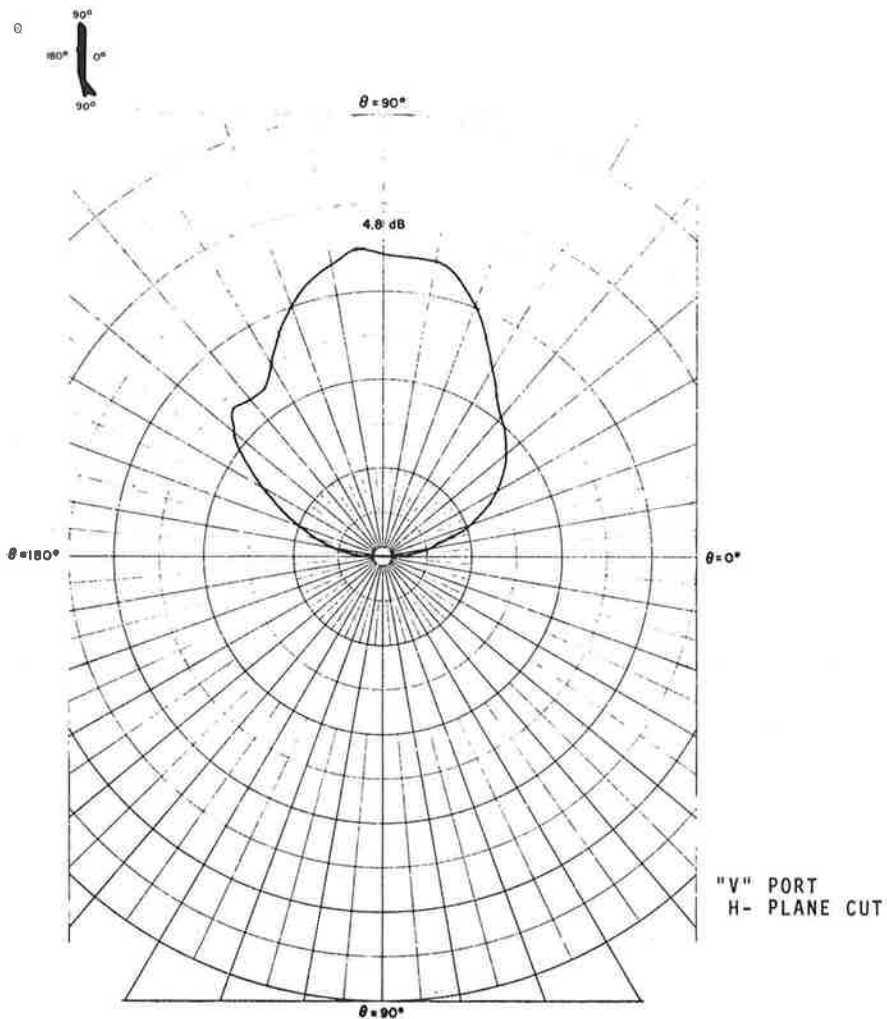CURVE PLOTTED IN VOLTAGE

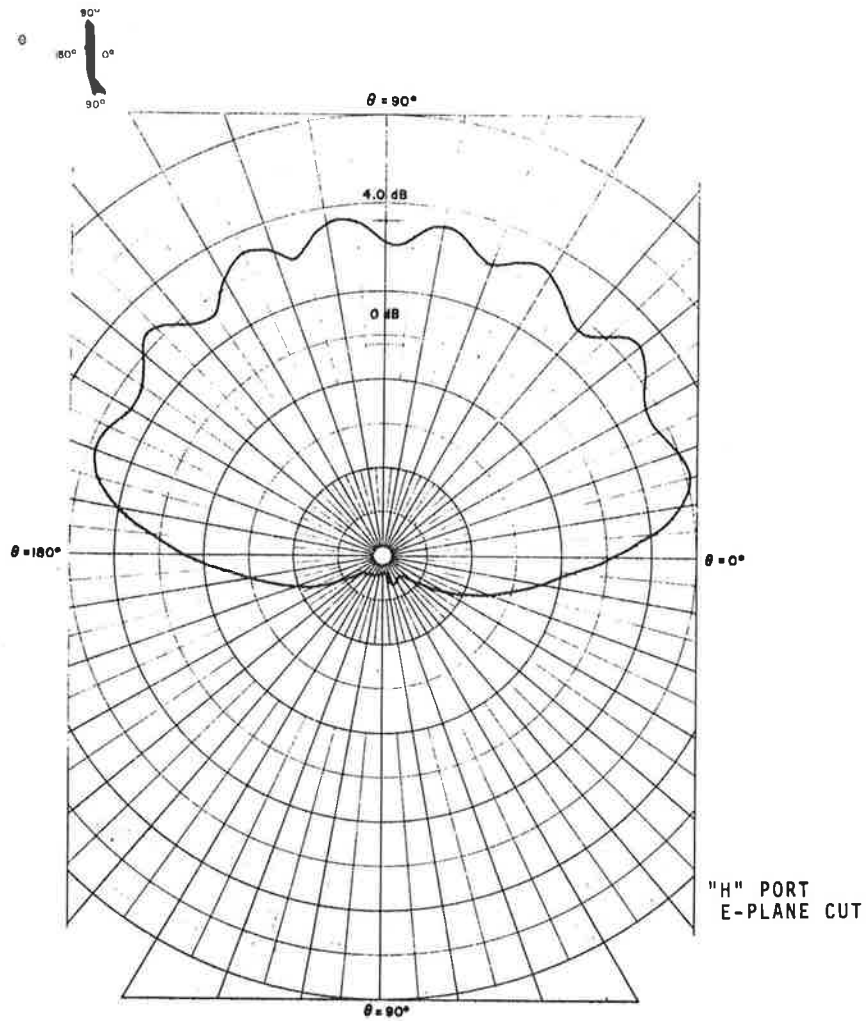Figure 35.   Full-Scale Antenna Pattern   "H" Port H-Plane Cut

64

PLANE TYPE_____MODEL SCALE FULL_____
ANTENNA TYPE_ORTHOGONAL MODE CAVITY_____
ANTENNA LOCATION_4 FOOT SQUARE GROUND PLANE
FULL SCALE FREQUENCY_1600 MHZ_____

VARIABLE ANGLE φ( ), θ(√)
CONSTANT ANGLE   φ═ 90 θ=___
POLARIZATION Eφ( ), Eθ(√)___
CURVE PLOTTED IN VOLTAGE

Figure 36.   Full-Scale Antenna Pattern   "H" Port H-Plane Cut Cross-Polarized

65

8. DIAMOND L-BAND ANTENNA

This is a description of the Diamond Model DIC-6980 Cavity Backed Dipole Fed Slot Antenna developed by Diamond Antenna & Microwave Corporation, of Winchester, Massachusetts, to obtain coverage characteristics for flush-mounted L-band (1535 - 1660 MHz) aircraft antennas.

8.1 ANTENNA ELEMENT LOCATIONS

The antennas were located as shown in Figure 37 as follows:

Forward of wings, Station 422.8, $\theta = 78°$ down from zenith on port side of fuselage.

Station 422.8 $\theta = 78°$ from zenith on starboard side of fuselage. Midway over wings, Station 803.5

    a)   Dorsal antenna facing $\theta = 0°$ (zenith)

    b)   Port antenna facing $\theta = 35°$

    c)   Starboard antenna facing $\theta = 35°$

Near trailing edge of the wings, Station 940

    a)   Dorsal antenna facing $\theta = 0°$

    b)   Port antenna facing $\theta = 35°$

    c)   Starboard antenna facing $\theta = 35°$

coordinates for antenna location are defined as the direction of the outward normal from the element aperture, and are consistent with the spatial angles in the aircraft/ pattern coordinates system (Figure 38).

Because of symmetry about the roll axis, only five antenna locations were used in the tests.

8.2 ANTENNA ELEMENT DESCRIPTION AND ORIENTATION

The antenna element is a cavity-backed dipole fed slot antenna as shown in Figure 39. The elements were oriented in the

ANTENNAS

STA 422.8

STA 803.5

STA 940
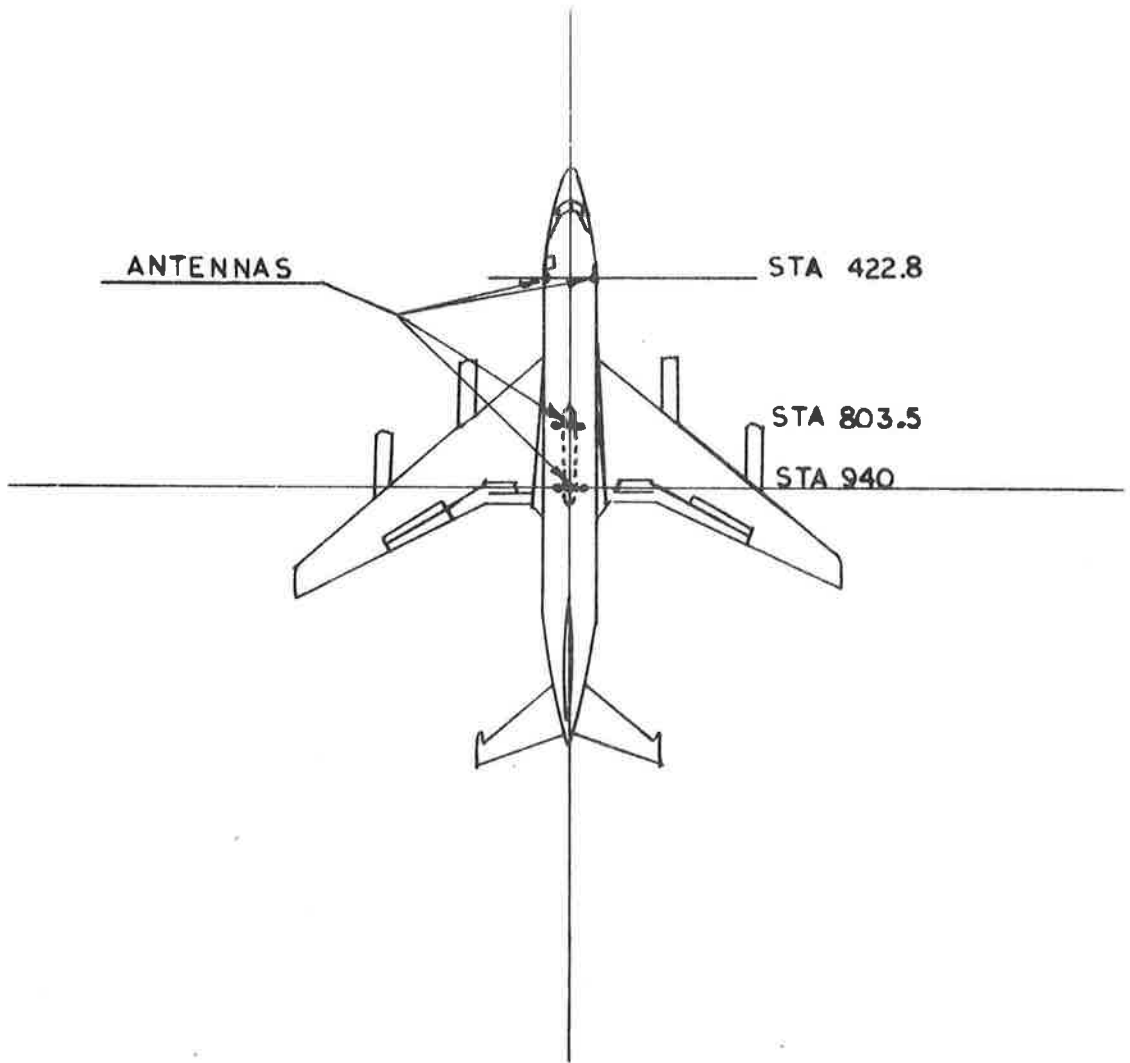
Figure 37. Antenna Element Locations
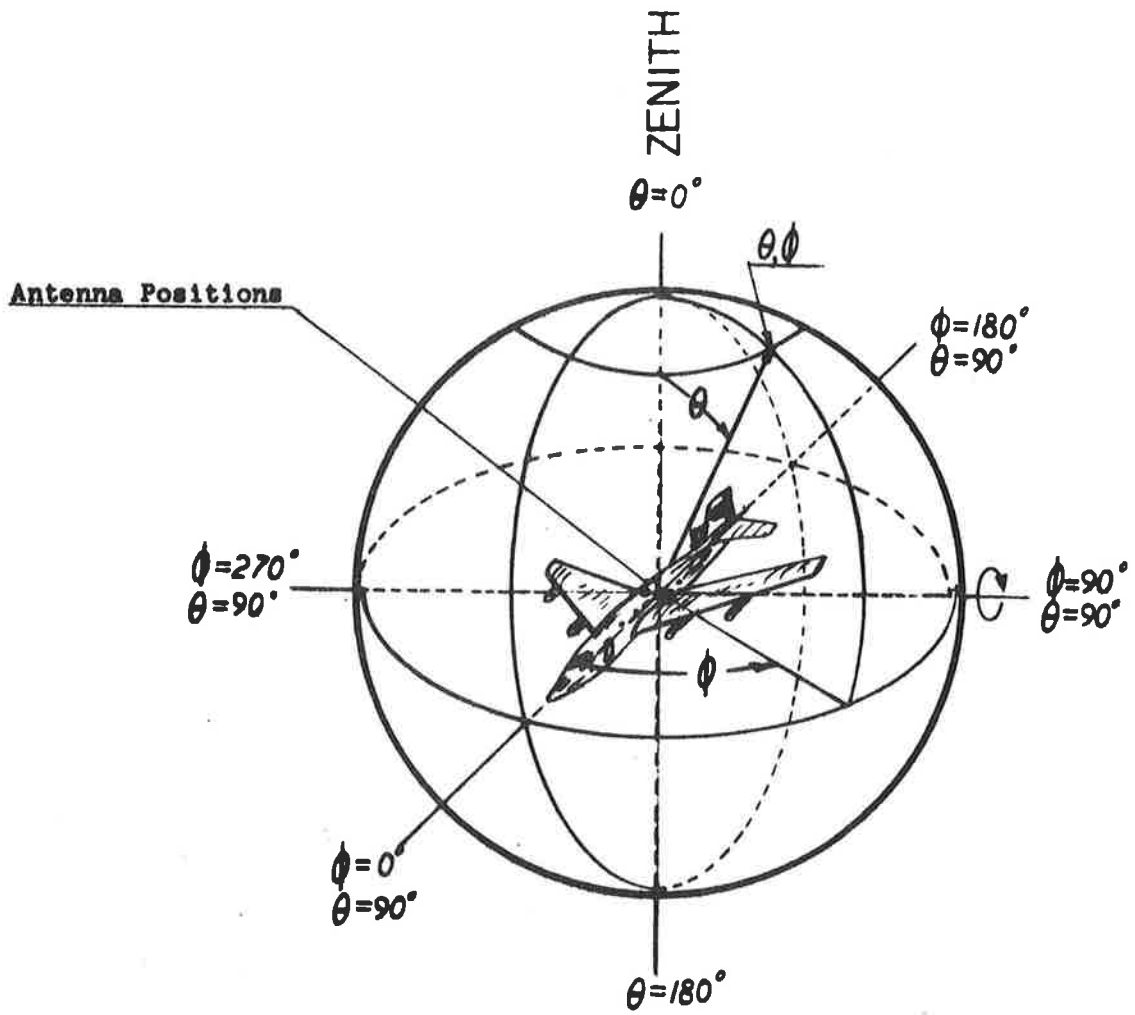
Figure 38. Antenna and Aircraft Coordinate System
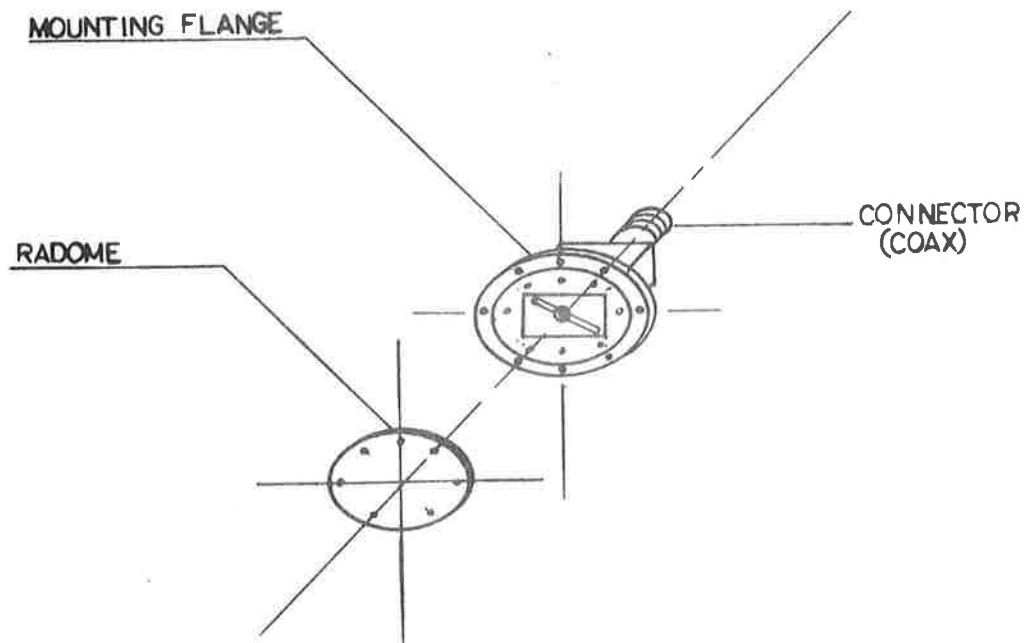
Figure 39. Antenna Element Description Dipole Slot

the aircraft with the slot length dimension orthogonal to the
fuselage roll axis (Figure 40). This particular element was se-
lected because of its broad coverage in circular polarization with
low axial ratios at wide angles from the beam maximum.

8.3 MEASURED PATTERNS

Relative power in decibels as shown in Figures 41 detail
a, b, c, and d for the antenna element located at Station 803.5
facing θ = 35° down from Zenith. Test patterns illustrate the
data measured in the following principal planes of the model air-
craft:

Figure 41a - Pattern in pitch plane of aircraft, $\emptyset$ = 0°, 180°,
θ = variable.

Figure 41b - pattern in roll plane of aircraft, $\emptyset$ = 90°, 270°,
θ = variable.

Figure 41c - Conical pattern in yaw plane of aircraft,
θ = 90°, $\emptyset$ = variable.

Figure 41d - Conical pattern at θ = 30°, and $\emptyset$ = variable.

Comprehensive data for five locations of the elements on the
fuselage are shown.[1] Peak gain values for the elements are on the
order of 8.0 dB above a circularly polarized isotropic radiator.

8.4 DISCUSSION OF DATA

8.4.1 Great Circle Patterns (Figures 41 Detail a and b)

There are obvious regions of pattern scintillation in the
direction of the vertical stabilizer and the tail of the aircraft.
The principal maximum of the pattern lobe occurs in the region of
θ = 35°, $\emptyset$ = 90°, which is the direction that the aperture is
facing on the port side. In the general direction of the wings
($\emptyset$ = 90° to 110°) and the side of the fuselage ($\emptyset$ = 110° to 170°)
the pattern asymmetry is quite evident, with fluctuation in gain
up to 3 dB caused by the reflection of waves from the aircraft
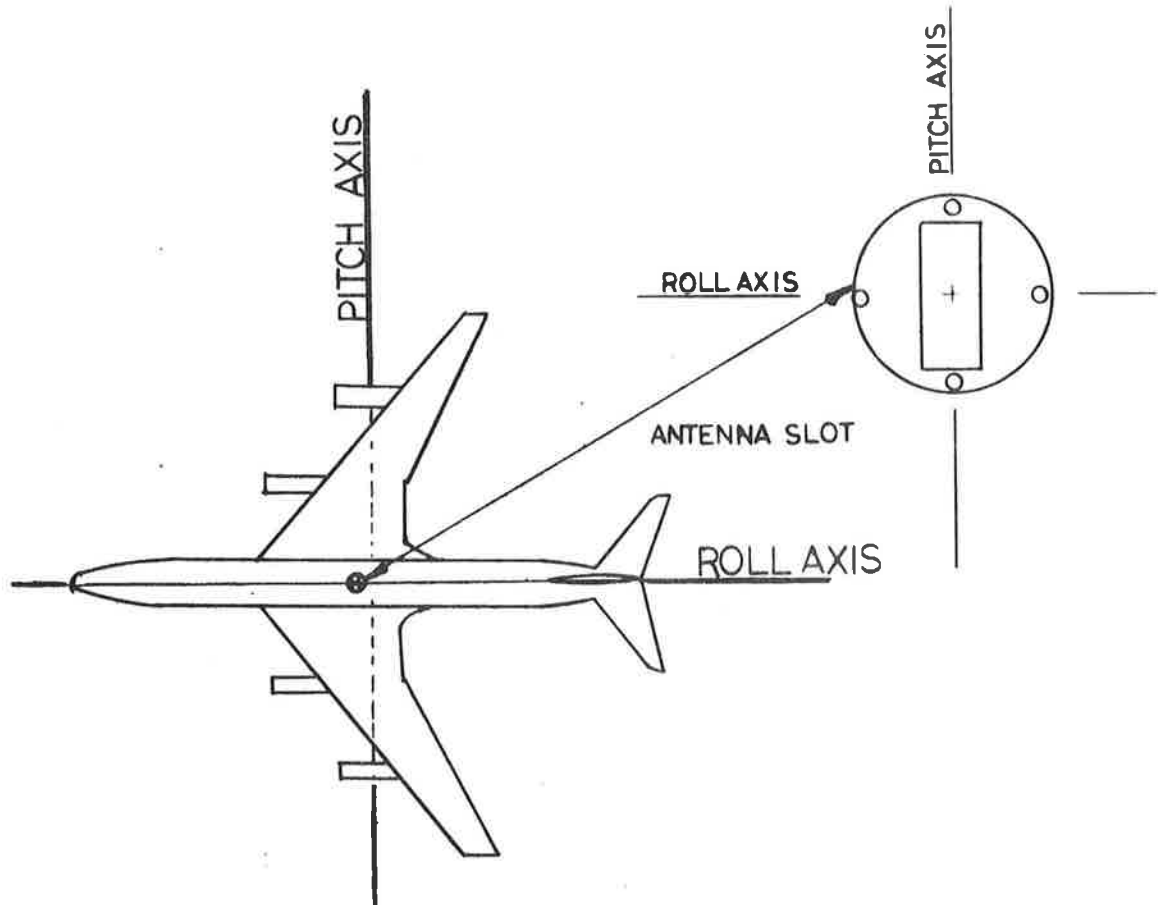
Figure 40. Antenna Element Orientation for Broad Coverage in
Pitch Plane of Aircraft

(a)

(b)
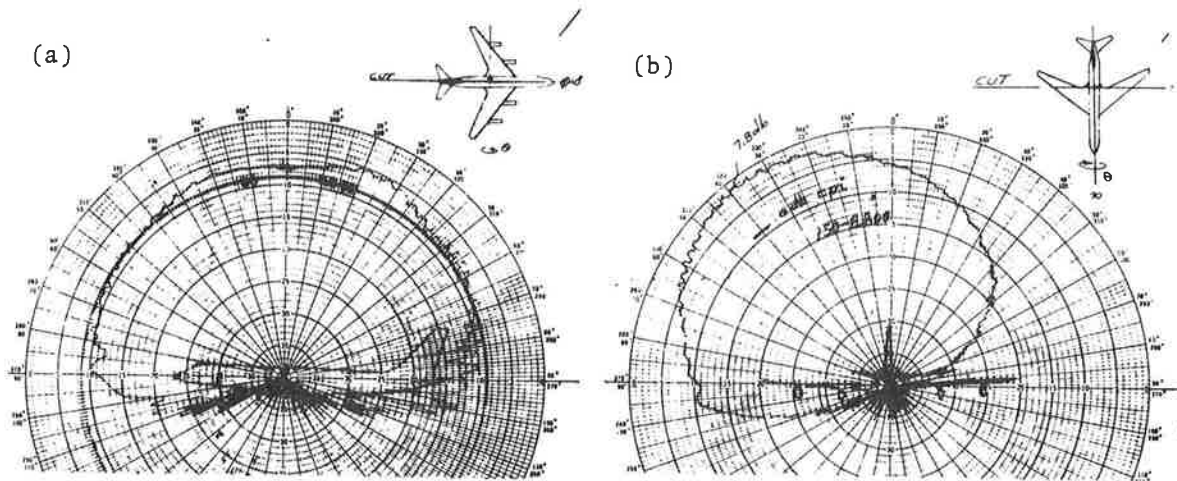
GREAT CIRCLE PATTERN POLAR DIAGRAMS

ANTENNA LOCATION - STATION 803.5
PORT SIDE - 35° DOWN FROM ZENITH
TRANSMITTER POLARIZATION - RHC
FREQUENCY - 15.5 GHz

(c)

(d)
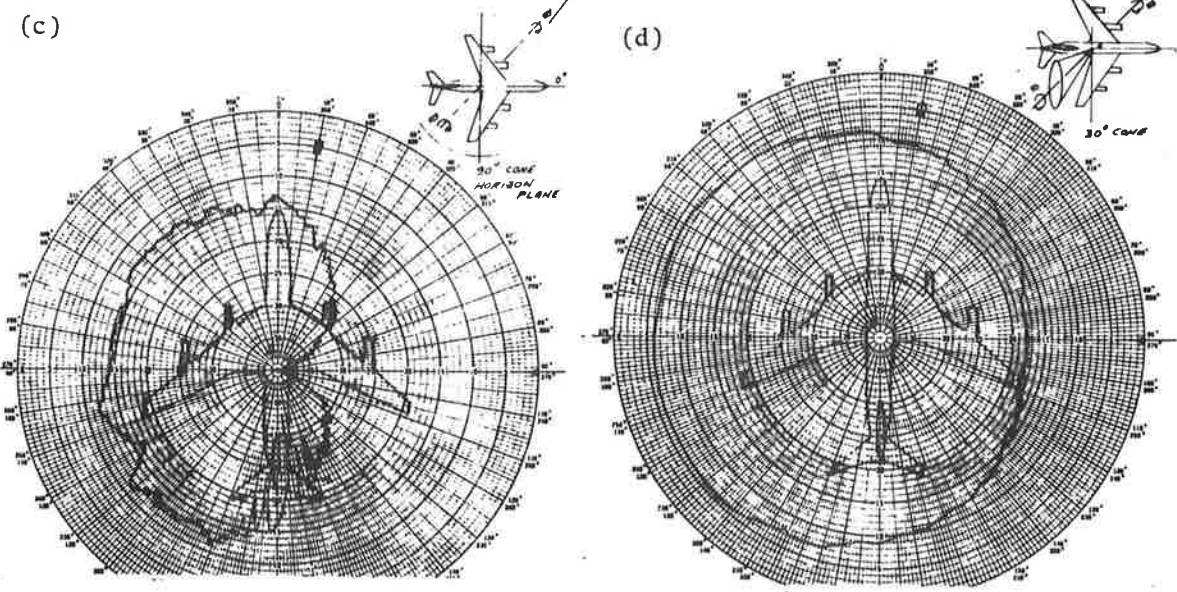
CONICAL PATTERN POLAR DIAGRAMS
ANTENNA LOCATION - STATION 803.5
ANGULAR LOCATION FROM ZENITH - 35°
TRANSMITTER POLARIZATION - RHC
FREQUENCY - 15.5 GHz
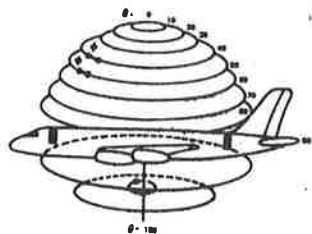
Figure 41. Principal Plane Patterns

72

structure on the port side of the model. The phase of the reflected electric fields is varying relative to the phase of the waves directly from the transmitter causing the resultant reinforcement and reduction of the pattern level. This rippling effect is quite evident on the pattern sheets for $\phi = 90°$ through $\phi = 170°$ in the regions defined by $\theta = 30°$ down to $\theta = 90°$ on the port side.

8.4.2 Conical Cut Patterns (Figures 41 Detail c and d)

In the regions close to zenith ($\theta = 0°$), the pattern is relatively smooth. At conical angles moving down closer to the horizon the obvious asymmetry of the patterns becomes evident. This is to be expected because of the asymmetric location of the antenna element on the port side of the model aircraft. Along the horizontal plane ($\theta = 90°$, $\phi = 120°$) in the direction of the wing on the port side, a null begins to occur. This null becomes quite deep and pronounced at $\theta = 100°$ (the 10° cone below the aircraft).[1] For $\theta = 110°$ there is an almost complete null.[1]

8.4.3 General Coverage Characteristics

There are two principal radiation lobes below the aircraft,[2] in the port side region bounded by the side of the fuselage forward of the wings and the leading edge of the wings, and a region between the trailing edge of the wing and the aft side of the fuselage. Below the horizontal plane of the aircraft on the starboard side, there is little or no radiation. At angles between $\theta = 130°$ and 180° (nadir), the pattern levels were approximately 30 dB below the peak, or greater, consequently they were considered negligible and not measured.

8.5 CONCLUSIONS

Element patterns and coverage are affected by location. Antenna elements installed on top of the fuselage centrally located between the leading and trailing edges of the wings have less coverage below the aircraft when compared to the coverage measured from antenna elements installed at the aft location nearer to the trailing edge of the wings. To suppress the effects of multipath the forward antenna location is more favorable.

Zenith antennas, i.e., those with apertures facing straight up above the aircraft, will provide smooth interference-free coverage from zenith $\theta = 0°$ down to $\theta = 45°$. At lower angles ($\theta = 45°$ to below the aircraft) the effects of the aircraft are indicated by pattern nulls in the direction of the wings, and severe pattern ripple in the direction of the vertical and horizontal stabilizers. The pattern lobe breaks up drastically near the horizon for the antenna elements installed in the port or starboard side of the fuselage.

8.6 RECOMMENDATIONS

The use of flush-mounted single element radiators in an aircraft will be useful for future air traffic control and communications systems if moderate gain (6 to 8 dBi) is satisfactory to produce acceptable performance in the receiving systems. The signal to noise ratios, false alarm rates, and detection probabilities must be determined in terms of state of the art and future transmitter powers and receiver sensitivities. The long-range routes and flight attitude of the aircraft must also be considered in a solution to determine the required antenna coverage. Consequently, a communications link analysis is recommended. This analysis will synthesize an antenna aperture for a required gain.

These recommendations are based on a critique of those methods used by systems engineers, in which the aircraft antenna coverage

74

is presupposed to be omni (0 dB) or moderate gain (3 to 6 dB) and then the signal to noise margins are determined. The directive gain required as a function of the aircraft coordinate spatial angles must be established for future systems.

Generally, antenna elements with broad coverage or arrays mounted on the tip of an aircraft fuselage may provide unperturbed directive beams for small angles near the zenith. Attempts to tilt or scan beams down close to the horizon will result in degradation of the gain function. Consequently, it is recommended that aircraft antenna elements and arrays be investigated to determine optimum locations on the aircraft which are consistent with the overall communications link scenarios.

Obviously, an antenna that should radiate a beam straight up should not be mounted on the underside of the fuselage or below the wings. In future systems, the required coverage direction may be off the tail, which will negate the use of forward or dorsal located elements. The antennas could then be installed facing aft. Ultimately, switching from element to element, or electronically scanning a beam must be considered, but the required aperture must be synthesized first from a theoretically required gain function. The implementation of hardware and the feasibility of producing systems should follow.

8.7 REFERENCES

1. McCabe, W.J., A Scale Model Aircraft and Antenna Pattern Test Program, Final Report on Contract No. DOT/TSC-167, October 1971, Diamond Antenna and Microwave Corporation, 33 River Street, Winchester, MA.

2. Balloons Used in Aerosat Tests; Aviation Week and Space Technology, Vol. 94, No. 25, June 21, 1971.

9. TEXAS INSTRUMENTS AIRBORNE ARRAY ANTENNA

Texas Instruments has recently completed a contract with the Air Force Avionics Laboratory to design and develop an airborne phased-array communication system.[1] The phased arrays used are linear arrays of square spiral elements. The elements in this case were designed for minimum thickness, with cavity depths of 0.1 inch to provide external aircraft mounting.

Cavity-backed Archimedian spiral antennas, both square and round, are excellent array elements from the standpoint of ellipticity ratio, beamwidth, and symmetry. These elements are inherently broadband devices. A great deal of experimental and analytical work has been performed on spirals, and Texas Instruments has performed numerous tests on these elements, both for broadband and phased-array purposes.

Texas Instruments has proposed this array to FAA for the Aerosat Program.[2] The proposed antenna is an 8-element linear array. The array is subdivided into two subarrays of 4 elements each for automatic steering. The array is to be capable of transmitting circular polarization. The transmit center frequency is 1650 MHz while the receive frequency is 1550 MHz. A square, cavity-backed spiral element is proposed for the array. Two antenna systems will be employed, one on each side of the aircraft.

Associated with each antenna element is an active electronic module. Each electronic module contains a diplexer, transmitter power amplifier, and lo-noise receive amplifier. Phasing circuitry is also included. The electronic module is placed immediately adjacent to the antenna element to maximize both the radiated RF power to input DC power ratio and the gain to noise temperature ratio of the communications system. Graceful degradation is also achieved since a single failure in any of the electronics modules does not degrade the system appreciably.

The element size is 3.7 inches square, or slightly less than 0.5λ. With this element spacing, the array is limited to a scan of

±60 degrees before the appearance of a grating lobe. The square spiral has good axial ratio performance over wide scan angles. Spirals may be loaded on the edges with a resistive material or lumped element resistor to eliminate energy reflected from the ends of the spiral arms' resistors giving the best loss performance. This loading improves the element's axial ratio. The element is fed with a stripline balun to provide suitable amplitude and phase excitation of the spiral over the operating frequency band. Spiral elements developed by Texas Instruments in this frequency range have yielded gains between 3.5 and 5 dB. The proposed element will have a minimum gain of 4dB at the transmit frequency with some degradation at the receiving frequency. Table 7 summarizes the performance characteristics of the proposed antenna element.

TABLE 7   SQUARE-SPIRAL PROPOSED
PERFORMANCE CHARACTERISTICS

Element gain, 0°	4.0 dB
Gain, 40° (35)	2.0 dB
Axial ratio, 0°	<1.0 dB
Axial ratio, 40° (35)	<2.5 dB
Element Depth	$\approx \lambda/4$
Element Size	3.7 in^2

As the array is scanned from the broadside direction, the array directivity decreases. This is due to the physical decrease in apparent aperture size as the subtended angle increases and is proportional to cos θ, where θ is the angle measured from array broadside. Array gain differs from directivity by impedance matching effects, and resistive losses in spiral and balun. Since the gain of an N element array is roughly N times the element gain (assuming identical elements), then all gain degradation effects may be calculated from knowledge of the element field pattern (gain) and a knowledge of the mutual coupling between the elements.

Figures 42a and 42b show recordings of the received power at the output of the array as the fuselage section on which the array was mounted was rotated through 180 degrees of azimuth while the

Measured gain: ~8 dB
Curves plotted in dB
Scale: 1 dB/Div.
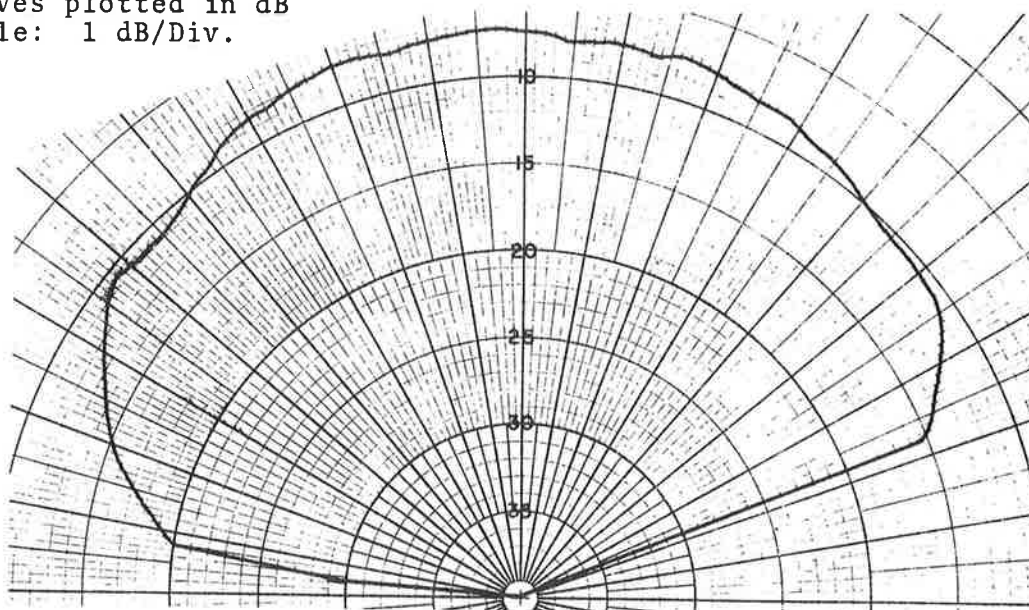
POLARIZATION - VERTICAL

Figure 42a. UHF Array in Auto-Track 1500 MHz (Vertical)

Gain at ±60-degree points: 5 dB below maximum gain
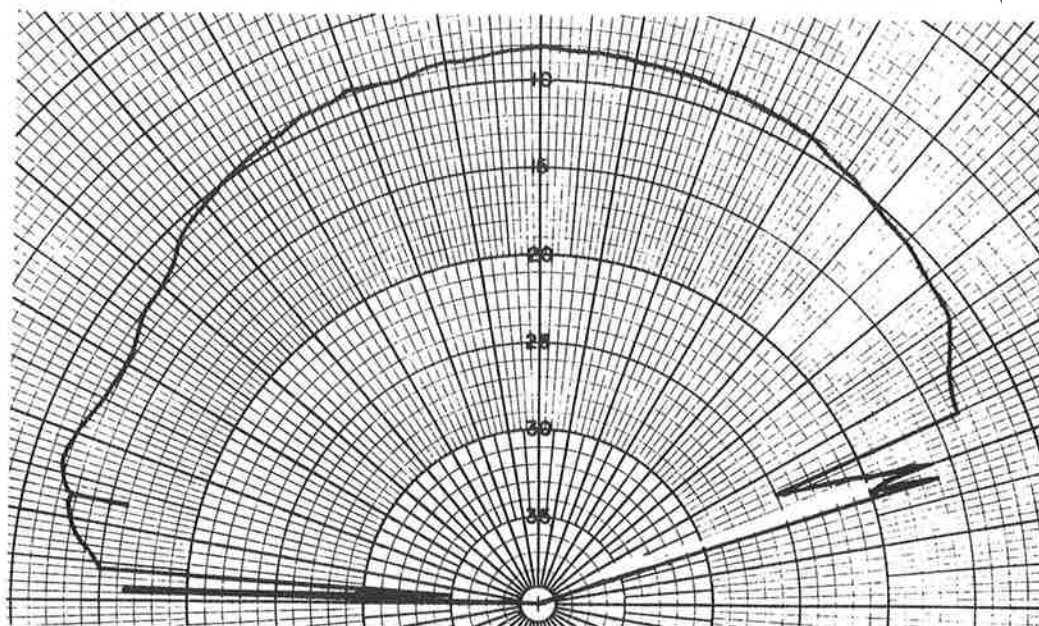
POLARIZATION - HORIZONTAL

Figure 42b. UHF Array in Auto-Track 1500 MHz (Horizontal)

78

antenna system, employing monopulse tracking, automatically maintained the maximum of the electronically formed beam on the targ⌐t. These curves were measured on Texas Instruments antenna range at Dallas as described in Technical Report AFAL-TR-70-136.

The array maintained lock on the target until the onset of grating lobes caused ambiguity to develop in the automatic steering circuitry. For the Air Force operational requirements, it was desirable to develop maximum gain (13.5 dB) at the expense of grating lobe formation. For Aerosat, however, it is possible to extend the range of automatic tracking by using a slightly smaller element and developing only 12.5 dB maximum gain but suppressing grating lobe formation to achieve automatic tracking operation to 10 degrees elevation.

For a C-135 aircraft to obtain the desired hemispherical coverage, two phased arrays have been proposed, one mounted on one side of the fuselage of the aircraft, and one mounted on the other, with the holes in the coverage optionally filled by additional fixed antennas in the radome and behind the vertical stabilizer. The coverage diagram for the two array case is shown in Figure 43. The array system specification is shown below.

Parameter	Value
Maximum EIRP (dBw)	34
Sidelobe Levels—Transmit (dB)	10
Maximum Transmit Gain (dB)	12
Coverage—Elevation (degrees)	– 30 to +90
Coverage—Azimuth (degrees)	115
EIRP at Extremities of Coverage (dBw)	29
Noise Temperature (°K)	540
Maximum Receive Gain (dB)	11.8
Gain-to-Noise-Temperature Ratio (dB/°K)	– 15.7
DC Power Input (watts)	600
Array Input Frequency (MHz)	1645 to 1660
Array Output Frequencies (MHz)	1543.5 to 1558.5
Number of Input RF Lines (50 Ω)	1
Number of Output RF Lines (50 Ω)	2
DC Voltages (volts)	+5, +28, +15
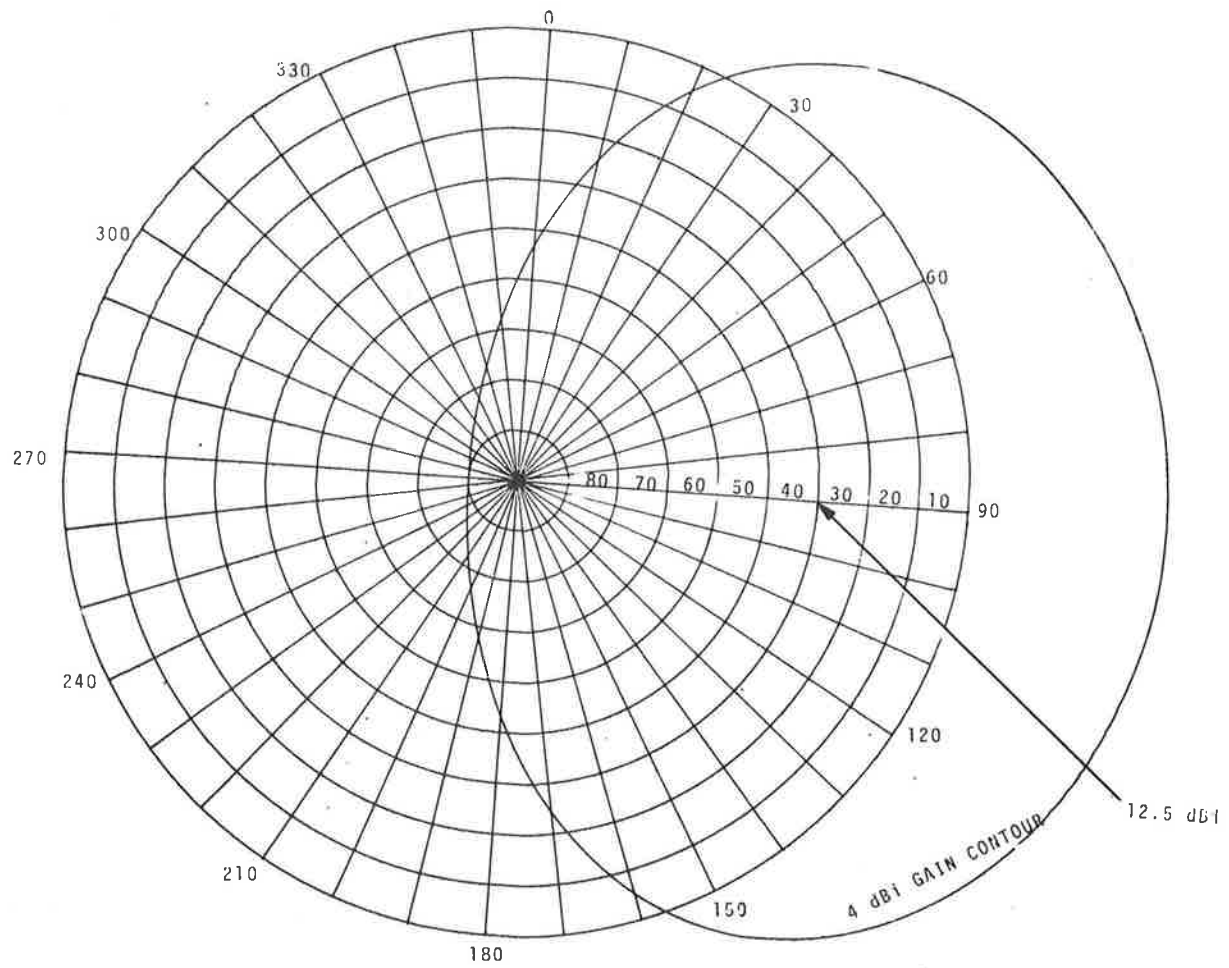
Figure 43. Azimuth/Elevation Contour of Coverage for 4dB: Minimum Gain--Antenna Boresight 12 Degrees above Horizon--8-Element Linear Array

80

9.1 REFERENCES

1. Airborne UHF Adaptive Phased Array. Texas Instruments Incorporated (Contract with AFAL, F33 (615)-1-706).

2. Development of a Moderate Gain L-Band Antenna System. Texas Instruments Inc. (Proposal to FAA, SP23-GP70). 1970.

10. DIOSCURES L-BAND ARRAYS

One antenna of this type is the Dioscures antenna (see Figures 44 and 45) which has been developed by ELECMA of France. Electrical characteristics are displayed in Table 8.

TABLE 8 ELECTRICAL CHARACTERISTICS OF
DIOSCURES ANTENNA

1. Minimum Gain Over the Principal Flight Route: 10 dB

2. Beamwidth (at -3 dB): 20° to 25° (Elevation)
                           40° to 45° (Azimuth)

3. Number of Beam Positions: 14 (Elevation
                               17 (Azimuth)

4. Beam Step Angel: ≈6° (Elevation)
                      ≈11° (Azimuth)

5. Total Coverage: 5° to 90° above horizon (Elevation
                     -90° to +90° from a beam (Azimuth)

6. Dimensions: Width: 19.5 in.
                 Height: 17.0 in.
                 Depth: 8.2 in

Each antenna, port or starboard, is composed of a convex array of radiating elements. This array comprises two sub-arrays of 7 elements oriented in such a way that each of the sub-arrays provides half the coverage. Each radiating element is formed of a crossed dipole associated with a 3 dB coupler forming the right and left circular polarizations. For each polarization, a switching and power divider assembly enables the antenna to be fed by fraction of sub-arrays in order to optimize the gain for the deflection chosen.

VERTICAL

ANGLE OF INCLINATION

AERIALS

DIPOLES

(R/F UNIT)

(TRANSMITTER COAXIAL CABLE)
COAXIAL EMISSION
COAXIAL RECEPTION
(RECEIVER COAXIAL CABLE)

(TO COMPUTER)
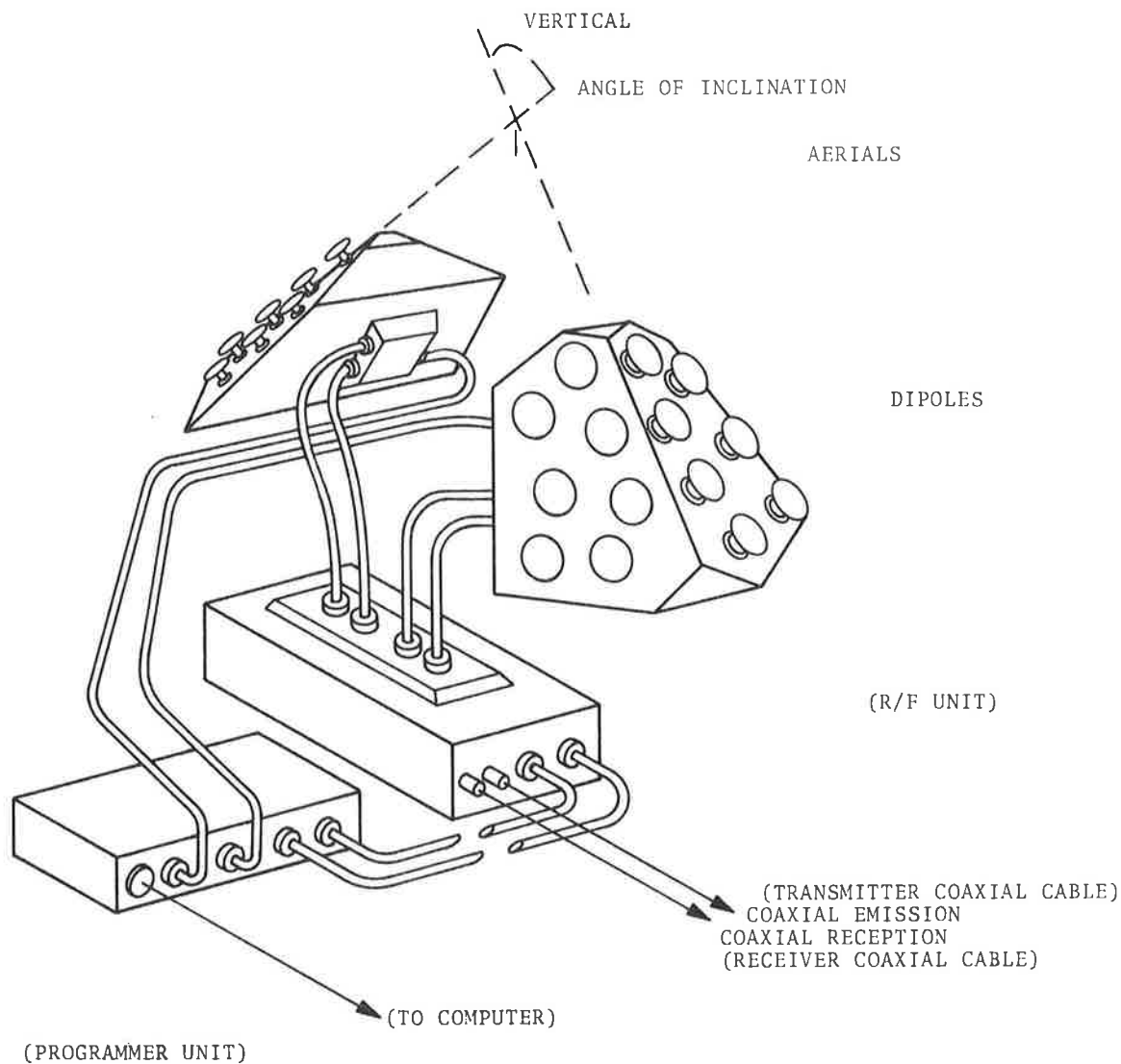
(PROGRAMMER UNIT)

THE TWO AERIALS AND THE RF UNIT ASSOCIATED
WITH THE PROGRAMMER

Figure 44.   L-Band Array (Dioscures)

POLES CROISES ET COUPLEURS 3dB
CROSSED DIPOLE WITH 3dB COUPLEUR

POLARISATION   (SATELLITE 2)
CIRCULAIRE GAUCHE

LEFT HANDED   (SATELLITE 2)
CIRCULAR POLARIZATION

COMMUTATEURS DE PANNEAUX

ANTENNA PANEL SWITCH

POLARISATION
CIRCULAIRE DROITE

RIGHT HANDED
CIRCULAR POLARIZATION

C^{de} DU 1er
FAISCEAU
(SATELLITE 1)

DIVISION DE PUISSANCE ET COMMANDE
DU BALAYAGE ELECTRONIQUE

POWER DIVISION AND ELECTRONICALLY
DESPUN CONTROL

VERS ANTENNE
BABORD

TO PORT
ANTENNA

1^{rst} BEAM
CONTROL
(SATELLITE 1)

PROGRAMMEUR

PROGRAMMER

VERS C^{de}
FAISCEAU 2
TO 2nd BEAM
CONTROL

DIPLEXEUR 1

DIPLEXEUR 1

SAT 1
CD POLARISATION
RH POLARIZATION

SAT 2
CD POLARISATION
RH POLARIZATION

VERS EMETTEUR

TO TRANSMITTER

C   C   C

COMMUTATEUR DE
PREAMPLIFICATEUR
PREAMPLIFIER
SWITCH

ALIMENTATION

POWER SUPPLY

P   P   P

PREAMPLIFICATEUR
PREAMPLIFIER

C   C   C

CALCULATEUR

COMPUTER

PANNEAU DE C^{de}

CONTROL PANEL

VERS RECEPTEURS

TO RECEIVERS

CAP

ROULIS
ROLL ANGLE

POSITION DE L'AVION
AIRPLANE POSITION

SYNOPTIQUE DE L'ANTENNE TRIBORD

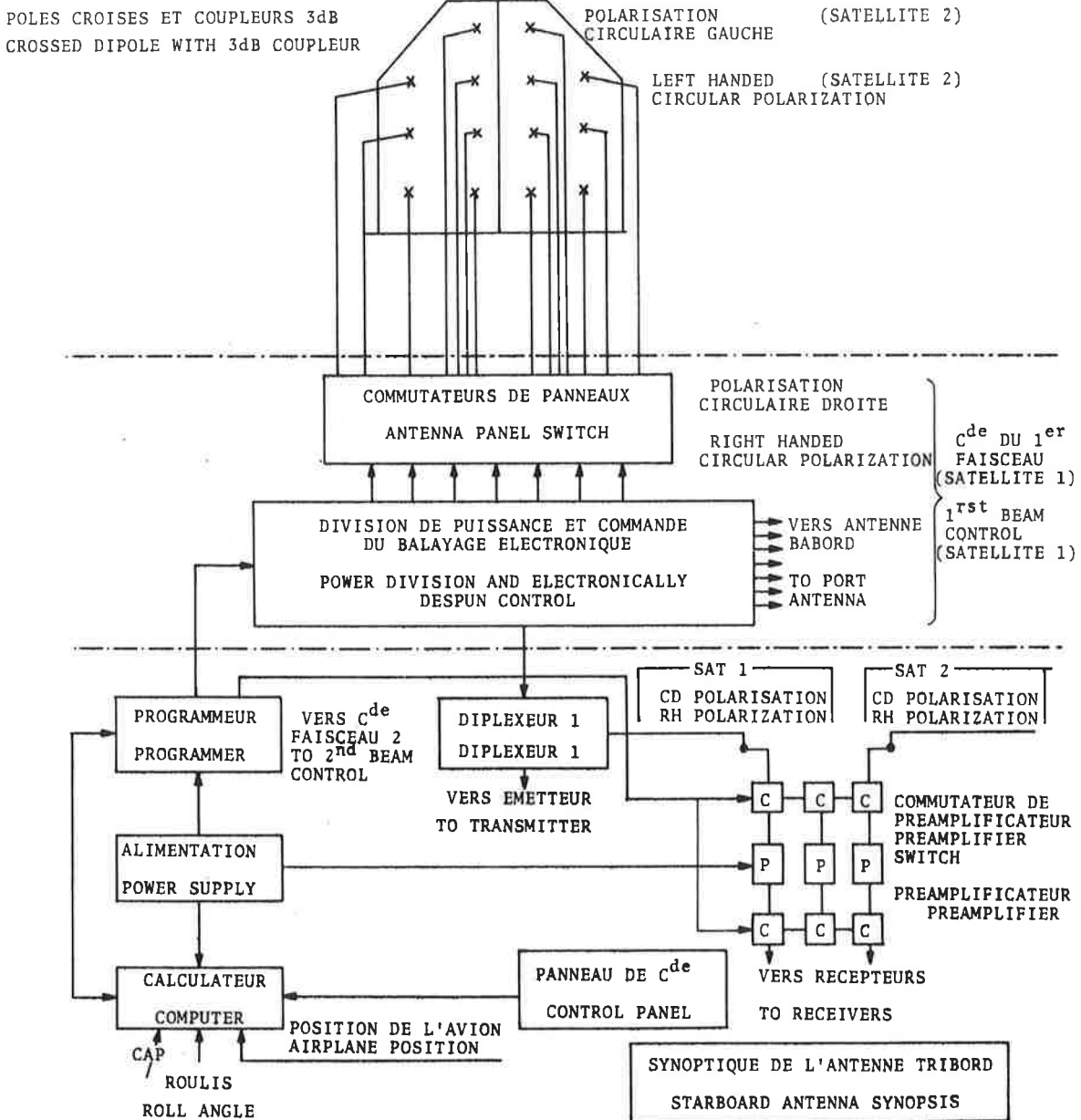STARBOARD ANTENNA SYNOPSIS

Figure 45.   L-Band Array (Dioscures)

84

totality as a single integrated system, and there is no reason why a fully digital system is not feasible. With the liberal use of integrated circuit technology and LSI, a single computer on-board the aircraft could provide the functions of navigation, communications, and status reporting. Furthermore, trends show that the cost of digital systems continues to decrease and, in the future, a fully digital system may become very cost-effective. Thus, a more detailed analysis of the projected cost of ownership of a hybrid system versus a fully digital system is needed to evaluate the true cost of ownership and performance associated with both systems.

The signals energizing the various radiating elements have phases reconstituting a wavefront perpendicular to the direction of the satellite with which the aircraft is in liaison.

The antenna requires a pointer which comprises:

1) A pointing computer which determines the direction of two satellites in a system of axes linked to the antenna from approximate position information of the aircraft and from the heading data; the aircraft roll data are also in-troduced into the computer to compensate for the aircraft's "rolling" movements around the roll axis;

2) a programmer which generates the phase control orders of the phaseshifters and the switching orders from angular coordinates of the directions in which the beams are pointing.

The major difficulties with this type of antenna are its high cost and complexity of operation; i.e., it requires either manual or electrical beam steering.

10.1 REFERENCE

1.   Dioscures Project 1972-1985. Global Satellite System for Telecommunications, Air Traffic Control, and Navigation. CNES, SGAT, July 1969.

11. PERFORMANCE OF AVAILABLE VOICE MODEMS

The following data were extracted from the final report 'Voice Coding and Intelligibility Testings for a Satellite Based Air Traffic Control System', April 1971, by J.N. Birch and N.R. Geizin of the Magnavox Company. This report was prepared for NASA, Goddard Space Flight Center.

Table 9 summarizes their findings for the voice coding techniques with regard to bit rate, size, weight, cost, power, performance, etc. These parameters are considered sufficient to interrelate the performance of these systems.

It is obvious from Table 9 that the choice of the appropriate voice coding technique for air traffic control depends upon the final system design. The choice would depend on whether the system is all-digital or whether a mixture of analog and digital information is transmitted. Digital systems have one advantage; i.e., they can be regenerated, transmitted via wireline, and improved by forward error control techniques. On the other hand, modems for wireline and forward error control devices cost additional monies and, therefore, increase the price of a single voice channel commensureately. If a hybrid system consisting of analog and digital signals is the ultimate design for the air traffic control, one tends to commend the analog transmission systems, since they are very cost-effective and economical of space, weight, and power requirements. Furthermore, the performance, based on published data, meets the requirements for sustaining voice circuits at low C/N_o values. They do not exhibit a thresholding effect peculiar to digital systems such as PCM, AΔM, and the vocoders. Furthermore, their reliability is inherently high because of their simple design. The basic limitation imposed on the analog systems is their inability to be regenerated. Both the adoptive NBFM and the Philips/LinCompex systems can be multiplexed in frequency, while the PDM can be multiplexed with other digital data in phase, time, or frequency.

Based on Table 9, it appears that for a hybrid ATC system, one consisting of a mixture of analog and digital signals wherein the voice is conveyed via an analog transmission, the best compromise approach for transmitting voice would be the Bell Aero's Adaptive Narrowband FM technique with the Magnavox PDM a strong second in this selection. With ANBFM as the prime means of conveying voice, digital data must be transmitted on a subcarrier or another independent carrier. While the measured intelligibility performance of ANBFM is better than PDM, based on data from the TSC-ESRO Tests of September, 1971, the fact that PDM can be easily multiplexed in time or phase with other digital data at little increase in cost is considered significant. When a data capability is added to ANBFM, the cost and bandwidth disparity with PDM no longer exists.

If, on the other hand, a fully digital system is desired, the all-digital vocoders operating at either 2.4 or 4.8 kbit/sec satisfy the 43 dB Hz design goal for sustained voice communication although their intelligibility is not as good as ANBFM. Vocoders which operate at 7.2 and 9.6 kbit/sec are at best marginal unless error control is employed to enhance their performance. Likewise, AΔM and PCM fall short of the design goal of 43 dB Hz, and the RF bandwidth limitation of 20 kHz does not provide enough bandwidth for error control enhancement. A typical forward error control equipment that could be used to make the digital systems perform at 40-43 dB Hz is the Viterbi algorithm convolutional encoder/decoder. This type of equipment costs at least $2000/unit but could insure a 4-5 dB system improvement, thus making the digital systems more competitive with the analog systems at low values of C/KT, while increasing the cost. Digital systems also require bit synchronizers and modems to disseminate the data, and the price of these devices should be included before a final system design can be meaningful.

At this point, it should be pointed out that the functions of air traffic control; namely, navigation, communications, and station-keeping, or status reporting, can be looked at in their

TABLE 9. COMPARISON OF VOICE-CODING TECHNIQUES

Voice-Coding Technique	Cost per Channel $	Size Cuin #	Wt #	Power Watts	Quality	Intelligibility (PB)	Reliability MTBF	Band-width	Avail-ability	Threshold of Perform	Multi-plex	Error Cont'l	Anti-Multipath	R&R	Constant Envelope
Adaptive FM	<500	VS	VS	VS	VG	95%	50,000	10 kHz	OTS	40 dB Hz	F	No	Yes	Yes	Yes
PDM	1500	300	15	10	VG	95%	20,000	20 kHz	OTS	"	FTθ	No	"	"	"
TI's Extended Range FM	?	VS	VS	VS	VG	95%	"	20 kHz	D	"	F	No	"	"	"
Phillip Co. (FRENA) Sincompex	1500	300	10	10	VG	95%	"	3-6 kHz	OTS	"	F	No	"	"	No
Analytic Rooter	1000	300	15	10	G	89%	"	1600 Hz	D	?	F	No	"	"	No
Channel Vocoder	5000	700	30	25	Fair	87%	5,000	2400 Hz	OTS	39 dB Hz	FTθ	Yes	"	"	Yes
Digital Vocoder	3000-4000	"	30	"	"	-90%	"	2400 Hz	OTS	39 dB Hz	"	"	"	"	"
Formant Vocoder	3000	300	15	15	"	89%	"	4800 Hz	D	42 dB Hz	"	"	"	"	"
4.8 Digital VEV	3000-4000	"	30	25	"	95%	"	"	OTS	42 dB Hz	"	"	"	"	"
7.2 - 9.6 VEV	4000	"	30	25	"	95%	"	9600 Hz	OTS	45 dB Hz	"	"	"	"	"
Censtrum Vocoder-Phase Vocoder 9.6 kbps	>15,000	?	?	?	"	95%	?	"	D	45 dB Hz	"	"	"	"	"
PCM Optimal Compander	500	VS	VS	VS	"	95%	50,000	20 kHz	OTS	48 dB Hz	"	No	"	"	"
Adaptive Delta Mod	500	VS	VS	VS	"	95%	"	"	OTS	44 dB Hz	"	No	"	"	"
Predictive Coding	10,000	?	?	?	"	95%	?	2400-9600 Hz	D	45 dB Hz	"	Yes	"	"	"
Modified Predictive Coding	2000	300	?	?	"	95%	?	9600 Hz	D	45 dB Hz	"	"	"	"	"

OTS - off the shelf   VG - very good   T - time

D - development   G - good   θ - phase

FTθ - Frequency-Time-Phase   F - frequency   VS - very small